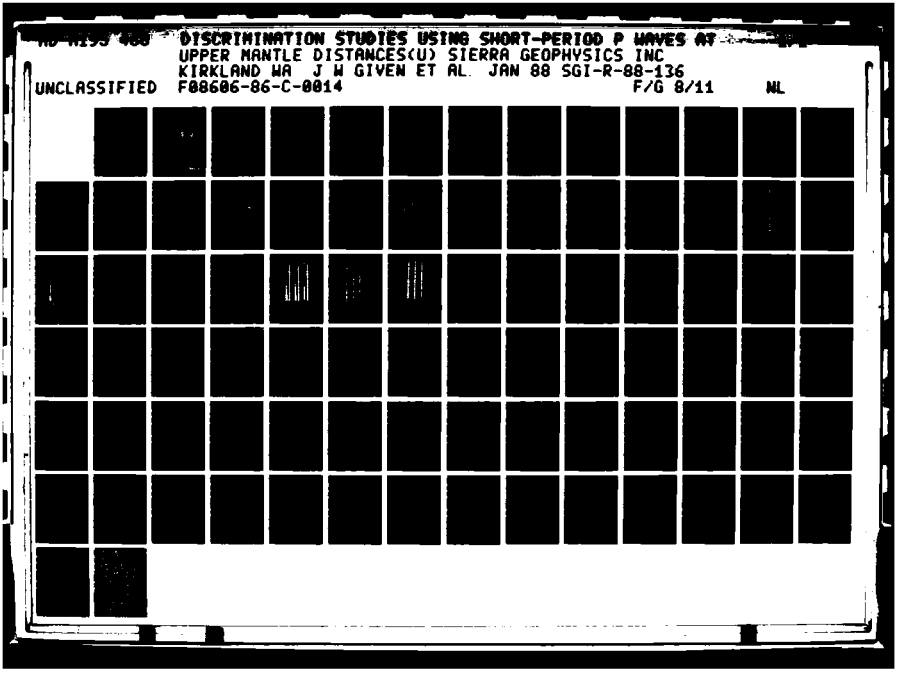
DISCRIMINATION STUDIES USING SHORT-PERIOD P WAVES AT
UPPER MANTLE DISTANCES(U) SIERRA GEOPHYSICS INC
KIRKLAND WA J W GIVEN ET AL. JAN 88 SGI-R-88-136
UNCLASSIFIED F08606-86-C-0014 F/G 8/11 NL

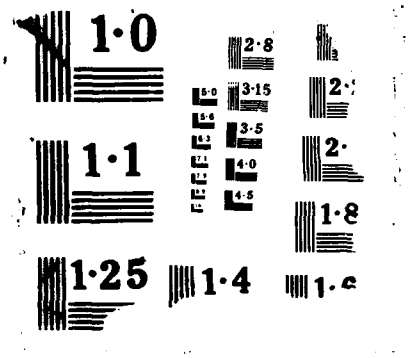
1·0
1·1
1·25
1·4
2·8
3·15
3·5
4·0
4·5
5·0
2·
1·8

(4)

SGI-R-88-136

DISCRIMINATION STUDIES USING SHORT-PERIOD P WAVES AT UPPER MANTLE DISTANCES

J.W. GIVEN
S.M. IHNEN
G.R. MELLMAN
W.C. TUCKER

SIERRA GEOPHYSICS, INC.
11255 KIRKLAND WAY
KIRKLAND, WA 98033

JANUARY 1988

ANNUAL REPORT
JANUARY 1986 - JANUARY 1987

The views and conclusions contained in this document are those of the authors and should not be interpreted as representing the official policies, either expressed or implied, of the Defense Advanced Research Projects Agency or the U.S. Government.

AIR FORCE TECHNICAL APPLICATIONS CENTER/TTR
HEADQUARTERS UNITED STATES AIR FORCE
PATRICK AIR FORCE BASE, FLORIDA 32925

Sierra

SPONSORED BY

DEFENSE ADVANCED RESEARCH PROJECT AGENCY (DoD)

AFTAC/TTR
REGIONAL DISCRIMINATION STUDY
ARPA ORDER NO. 4511, AMENDMENT 7
ISSUED BY AFTAC UNDER CONTRACT #F08606-86-C-0014

UNCLASSIFIED

SECURITY CLASSIFICATION OF THIS PAGE

REPORT DOCUMENTATION PAGE

1a. REPORT SECURITY CLASSIFICATION Unclassified	1b. RESTRICTIVE MARKINGS
2a. SECURITY CLASSIFICATION AUTHORITY	3. DISTRIBUTION/AVAILABILITY OF REPORT Approved for public release; distribution is unlimited
2b. DECLASSIFICATION/DOWNGRADING SCHEDULE	
4. PERFORMING ORGANIZATION REPORT NUMBER(S) SGI-R-88-136	5. MONITORING ORGANIZATION REPORT NUMBER(S)
6a. NAME OF PERFORMING ORGANIZATION Sierra Geophysics, Inc. 6b. OFFICE SYMBOL (If applicable) 4R088	7a. NAME OF MONITORING ORGANIZATION Air Force Technical Applications Center/TTR
6c. ADDRESS (City, State and ZIP Code) 11255 Kirkland Way Kirkland, WA 98033	7b. ADDRESS (City, State and ZIP Code) Headquarters United States Air Force Patrick Air Force Base, FL 32925
8a. NAME OF FUNDING/SPONSORING ORGANIZATION Defense Advanced Research Projects Agency 8b. OFFICE SYMBOL (If applicable) DARPA	9. PROCUREMENT INSTRUMENT IDENTIFICATION NUMBER F08606-86-C-0014
8c. ADDRESS (City, State and ZIP Code) 1400 Wilson Blvd. Arlington, VA 22209	10. SOURCE OF FUNDING NOS. PROGRAM ELEMENT NO. / PROJECT NO. DT6121 / TASK NO. / WORK UNIT NO.
11. TITLE (Include Security Classification) See Section 16	
12. PERSONAL AUTHOR(S) J.W. Given, S. Ihnen, G.R. Mellman, W. Tucker	
13a. TYPE OF REPORT Annual 13b. TIME COVERED FROM Jan. '86 TO Jan. '87	14. DATE OF REPORT (Yr., Mo., Day) 1988 January 15. PAGE COUNT 82
16. SUPPLEMENTARY NOTATION Discrimination Studies Using Short-Period P Waves at Upper Mantle Distances	
17. COSATI CODES FIELD / GROUP / SUB. GR.	18. SUBJECT TERMS (Continue on reverse if necessary and identify by block number) Discrimination, earthquake, explosion, upper mantle structure, Pearce processor

19. ABSTRACT (Continue on reverse if necessary and identify by block number)

Seismograms recorded at regional (1000 km) and upper mantle (1000 - 3000 km) distances are complex and variable due to the strong lateral and vertical heterogeneities in the seismic velocity structure. Thus, they are difficult to use in routine discrimination between earthquakes and explosions using the depth and focal mechanism discriminants that are useful at teleseismic (3000 km) distances. Yet the enhancement in the amplitude of seismic body waves at these distances due to closer proximity to the source and from focusing in the high velocity gradients in the upper 700 km of the mantle make it necessary to use these seismograms for monitoring low yield nuclear tests. In this report we review the properties of seismograms recorded at upper mantle distances in stable continental region such as northwest Eurasia in order to examine how well current models predict the general behavior of the observations and to see how much unmodeled energy, or noise, is present. In general, we found that the proposed models for the region predict the major arrivals observed in the data. For explosions, there are few distinct arrivals that are not

20. DISTRIBUTION/AVAILABILITY OF ABSTRACT UNCLASSIFIED/UNLIMITED ☒ SAME AS RPT. ☐ DTIC USERS ☐	21. ABSTRACT SECURITY CLASSIFICATION Unclassified
22a. NAME OF RESPONSIBLE INDIVIDUAL Dr. Dean A. Clauter	22b. TELEPHONE NUMBER (Include Area Code) (305) 494-7665 22c. OFFICE SYMBOL AFTAC/TTR

DD FORM 1473, 83 APR EDITION OF 1 JAN 73 IS OBSOLETE.

Unclassified

SECURITY CLASSIFICATION OF THIS PAGE

associated with some predicted upper mantle phase. However, noise levels (or code amplitudes), are large, since each arrival has a code associated with it that adds constructively at the receiver.

Using predicted coda amplitudes, we investigate how to use these data in a Pearce algorithm to discriminate on the basis of focal mechanism. We have found that given good azimuthal coverage of an event (e.g., 3 of 4 quadrants), the observed complexity of the explosion seismograms is incompatible with that predicted for earthquakes at depth using simple models for the reflection of the depth phases pP and sP. These results are similar to previous findings that considered teleseismic data.

We have applied the Pearce algorithm to several North American events with good coverage at upper mantle distances to investigate the predictability of the short-period seismograms from earthquakes. For these events, the timing of the later arrivals in the seismograms are inconsistent with an explosion source. On the other hand, the timing and the relative amplitudes of the later arrivals are consistent with fault mechanisms that agree with published results.

To increase the effectiveness of the Pearce algorithm, we have attempted to develop methods to enhance the detection of the depth phases and determine the relative polarities. One promising method involves applying spiking filters to the autocorrelation of a seismogram. This process increases the resolvability of distinct arrivals in time and, thus, comparison of similarly processed seismograms to detect depth phases is made easier. The method seems to work well on seismograms with distinct arrivals and may prove useful in sorting out seismograms recorded at upper mantle distances where as many as 5 replications of the P, pP, and sP wave trains are expected.

TABLE OF CONTENTS

		PAGE
	LIST OF FIGURES	iv
1.0	SUMMARY	1
2.0	INTRODUCTION	3
3.0	OBSERVED SEISMOGRAMS AT UPPER-MANTLE DISTANCES IN NORTHWEST EURASIA	7
	3.1 OBSERVED P WAVES FROM 700 TO 1500 KM IN NORTHWEST EURASIA	17
	3.2 P-WAVE SEISMOGRAMS BETWEEN 1600 AND 4000 KM IN NORTHWEST EURASIA	23
	3.3 MODELING CONSIDERATIONS USING UPPER MANTLE SEISMOGRAMS	35
4.0	SYNTHETIC TESTS ON EXTENDING THE PEARCE PROCESSOR TO UPPER-MANTLE DISTANCES	37
5.0	PEARCE FOCAL SPHERE ANALYSIS OF TWO WESTERN U.S. EVENTS	45
6.0	CHARACTERIZING THE RELATIVE AMPLITUDES AND POLARITIES OF LATER ARRIVALS BY FILTERING THE AUTOCORRELATION FUNCTION	57
7.0	CONCLUSIONS AND RECOMMENDATIONS	65
8.0	REFERENCES	68
	DISTRIBUTION LIST	70

LIST OF FIGURES

		PAGE
FIGURE 1	Travel time curves for two upper mantle models for northwest Eurasia.	9
FIGURE 2	Two upper-mantle P-wave velocity models proposed for northwest Eurasia.	10
FIGURE 3	Location map showing station and event distribution for data discussed in this study.	12
FIGURE 4	Synthetic seismogram profile for model K8.	14
FIGURE 5	Synthetic seismogram profile for model KCA.	15
FIGURE 6	Observed seismograms from Soviet Peaceful Nuclear Explosions.	18
FIGURE 7	Observed short-period vertical seismogram at DWWSSN station KEV from Novaya Zemlya explosion.	19
FIGURE 8	Same seismogram as shown in Figure 7 except filtered with high pass filter at 4 Hz.	20
FIGURE 9	NORESS (NRAO) seismogram of Soviet explosion (PNE) on 18 July 1985. P_n and S_n phases are indicated.	24
FIGURE 10	First 30 s of 3 component NORESS seismogram shown in Figure 9.	25
FIGURE 11	NORESS seismogram from Figure 10 filtered at 4 Hz.	26
FIGURE 12	Seismograms from Novaya Zemlya explosion of 25 October 1984 recorded at NORESS (top, array sum) and KONO (bottom).	27
FIGURE 13	Sample of explosion data from Soviet tests and PNE's.	28
FIGURE 14	NORSAR array seismograms for Soviet PNE at 3160 km (to N1AO), 61°azimuth.	30
FIGURE 15	NORSAR array seismograms for Soviet PNE at 2894 km (to N1AO), 106°azimuth.	33

PAGE

FIGURE 16	Discrimination ability of the Pearce algorithm using one station, plotted as a function of take off angle.	40
FIGURE 17	Discrimination ability of the Pearce algorithm for stations at 20 and 40 degree P-wave take off off angle, plotted as a function of the number of stations.	41
FIGURE 18	Resolvability of depth phases pP and sP as a function of event depth and station distance.	43
FIGURE 19	Data and synthetics for the October 18, 1984, Wyoming event (lat. 42.38, lon. -105.72).	47
FIGURE 20	Vector plots of acceptable focal mechanisms as determined from the Pearce algorithm grid search for the Wyoming event.	49
FIGURE 21	Focal plane plots of the acceptable mechanisms for model 2 for the Wyoming event.	51
FIGURE 22	Data and synthetics for the October 29, 1983, Borah Peak, Idaho, aftershock of 23:29 (lat.44.23 lon. -114.11).	52
FIGURE 23	Vector plots of acceptable focal mechanisms as determined from a Pearce algorithm grid search for the Idaho event.	55
FIGURE 24	Synthetic example demonstrating how filtering the autocorrelation function enhances arrivals.	63
FIGURE 25	Seismogram, autocorrelation, and filtered autocorrelation for a MAIO recording of an East Kazakh explosion (19.8^{o}).	64

1.0 Summary

Seismograms recorded at regional (<1000 km) and upper mantle (1000 - 3000 km) distances are complex and variable due to the strong lateral and vertical heterogeneities in the seismic velocity structure. Thus, they are difficult to use in routine discrimination between earthquakes and explosions using the depth and focal mechanism discriminants that are useful at teleseismic (>3000 km) distances. Yet to monitor low yield nuclear tests, it is necessary to make use of the enhancement in the amplitude of seismic body waves at these distances due to closer proximity to the source and from focusing in the high velocity gradients in the upper 700 km of the mantle. In this report we review the properties of seismograms recorded at upper mantle distances in stable continental region such as northwest Eurasia in order to examine how well current models predict the general behavior of the observations and to see how much unmodeled energy, or noise, is present. In general, we found that the proposed models for the region predict the major arrivals observed in the data. For explosions, there are few distinct arrivals that are not associated with some predicted upper mantle phase. However, noise levels (or coda amplitudes) are large, since each arrival has a coda associated with it that adds constructively at the receiver.

Using predicted coda amplitudes, we investigate how to use these data in a Pearce algorithm to discriminate on the basis of focal mechanism. We have found that given good azimuthal sampling of the P waves from

an event (e.g. 3 of 4 quadrants), the observed explosion seismograms are incompatible with the pattern of later arrivals predicted for earthquakes at depth using simple models for the reflection of the depth phases pP and sP. These results are similar to previous findings that considered teleseismic data.

We have applied the Pearce algorithm to several North American earthquakes with good coverage at upper mantle distances to investigate the predictability of the short-period seismograms from earthquakes. For these events, the timing of the later arrivals in the seismograms are inconsistent with an explosion source. On the other hand, the timing and the relative amplitudes of the later arrivals are consistent with fault mechanisms that agree with published results.

To increase the effectiveness of the Pearce algorithm, we have attempted to develop methods to enhance the detection of the depth phases and determine the relative polarities. One promising method involves applying spiking filters to the autocorrelation of a seismogram. This process increases the resolvability of distinct arrivals in time and, thus, comparison of similarly processed seismograms to detect depth phases is made easier. The method seems to work well on seismograms with distinct arrivals and may prove useful in sorting out seismograms recorded at upper mantle distances where as many as 5 replications of the P, pP, and sP wavetrains are expected.

2.0 Introduction

The depth and focal mechanism of a seismic event are reliable, simple discriminants between earthquakes and underground explosions. However, these discriminants are currently most useful for detecting earthquakes below 15 km observed at distances beyond 25^{o}, which effectively limits their usefulness for detecting and discriminating the small shallow events of particular concern in monitoring low yield nuclear tests. To monitor small events, it is desirable to extend these discriminants to higher frequencies (> 5 Hz), nearer ranges (< 2500 km), and to shallower events (< 10 km). Thus it is of interest to examine wave propagation at regional (< 1000 km) and upper-mantle (1000 - 2500 km) distances in order to assess how to apply these discriminants for small events at these ranges.

A natural way to utilize these discriminants is to develop inversion methods that exploit as much information as is available in the seismograms to limit the set of probable source models as much as possible. Such an inversion algorithm was proposed and developed by Pearce in a series of reports (Pearce, 1977, 1979, 1980). In the Pearce algorithm, the observables are the relative amplitudes of the direct P waves and the surface reflections, pP and sP, along with the polarities of the direct and reflected phases. Thus, both the upgoing P and S portions of the focal sphere, as well as the downgoing P portion are sampled. Furthermore, S energy is used through the converted phase, sP, and so differences in P- and S- wave propagation

between the source and receiver are minimized (however the S to P reflection coefficient at the free surface may be subject to considerable uncertainty). The inversion method is a simple grid search over all possible earthquake focal mechanisms to determine the set of mechanisms consistent with all or some of the observations. If no reasonable mechanism is consistent with the observables, then the possibility that the event may be an explosion can be explored.

One advantage of this inversion approach is the enhanced confidence in the identification of depth phases. The depth of a seismic event is an important discriminant and the only reliable means of determining depth is by identifying the depth phases, pP and/or sP. Often, the surface reflections are obscured by radiation pattern effects. By examining systematic variations in pP and sP amplitudes with azimuth and distance, the observability of depth phases can be tied directly to the earthquake source mechanism.

Another advantage of the Pearce approach is that it can determine focal mechanisms without requiring the polarity data. Source mechanisms are typically determined by plotting P-wave polarities onto a spherical projection around the source and fitting nodal lines between polarity reversals. This traditional method is limited because for some mechanisms, such as thrust or normal mechanisms, the polarity reversals may be difficult to observe because the station coverage does not include any receivers near the nodal planes. Another factor limiting the usefulness of this approach is the signal to noise ratio.

Often, particularly at distances less than 25^{o}the first arrivals are emergent and the polarity may be impossible to determine. The detection of polarity has been sufficiently difficult that earthquake detection by observing dilatational first arrivals is not currently viewed as a reliable discriminant (Douglas, 1981). The Pearce method uses bounds on the relative amplitudes of P, pP, and sP to constrain the mechanisms and thus, there is an increased chance that data near a nodal plane (either P or S) is available. Furthermore, data near a nodal plane is indicated by a small relative amplitude of one of the phases in the P wave; thus, one station can provide valuable constraints on the position of a nodal plane.

The Pearce algorithm has been examined and extended by McLaughlin et al. (1983, 1985). Their analysis of several events has shown that typical observations of nuclear explosions at teleseismic (> 30^{o}) distances are not consistent with any earthquake focal mechanism at depths below 3 km, provided that data with good azimuthal coverage of the event is available. Futhermore, the method usually determines focal mechanisms that are consistent with the regional tectonic character, thus providing a tool for studying small events in remote regions where the tectonics are poorly known. McLaughlin et al. (1985) have extended the Pearce processor to formally account for errors and inconsistencies in the input observations, resulting in maximum likelihood determination of possible earthquake mechanisms. This is a valuable enhancement for routine application that eliminates the true or false criteria of the earlier Pearce algorithm.

The success of the Pearce technique depends on good azimuthal coverage of stations and tight constraints on the amplitudes of the depth phases. Although polarity information is not required, it can be included into the algorithm and provides very useful constraints on the possible mechanisms. Polarity information will be particularly important for detecting multiple explosions and thus it is useful to investigate processing methods that can determine relative polarities within a single seismogram or between several seismograms. Smart and McLaughlin (1985) have investigated ways of determining the relative polarity of pP and P waves from events at teleseismic distances. It is of interest to see whether these techniques can be extended to the more complex seismograms at regional and upper mantle distances.

In the following report, we will investigate how to extend the Pearce technique to upper-mantle distances. The initi l step is to review the observations of events recorded at upper-mantle ranges to examine the consistency of the later arrivals and the extent to which the seismograms can be deterministically modeled. We will examine how well short period data can be used to constrain focal mechanisms through some simple forward modeling experiments. Finally, we will present preliminary results on some processing techniques to enhance detection of later arrivals and determine their timing and relative polarity.

3.0 Observed Seismograms at Upper-Mantle Distances in Northwest Eurasia

Seismograms recorded at distances less than about 25^{o} are remarkably complex, indicating that there is considerable vertical and lateral heterogeneity in the upper mantle. Because the propagation complexity obscures many of the details of the source mechanism that are important for discrimination, the velocity structure of the upper mantle has been the subject of considerable research. Some features in the structure, particularly those associated with deeper structure such as the 400 km and 700 km discontinuities, appear to be ubiquitous; other properties, such as the low velocity zone and the attenuation of the uppermost mantle, vary from place to place giving rise to large variations in the appearance of regional and upper mantle seismograms. In this section we will review the observations of seismograms recorded between 700 and 3500 km in Northern Europe and Western Asia to examine their consistency and predictability in terms of some simple upper mantle models. The data will be primarily explosion data from the Soviet peaceful nuclear explosions in western Russia recorded at the northern European digital seismographs and the NORSAR and NORESS arrays. We will be particularly interested in how much of the complexity observed in the seismograms is actually predicted by the models and how much unmodeled energy or noise is present.

Complexity as a discriminant has not been emphasized recently (Douglas (1981). At teleseismic distances (> 30 deg.), seismograms from explosions usually appear simpler than earthquakes and several measures have been tried to quantify these differences in a way that will separate the populations. The discriminant fell out of favor with the observation of some complex explosion records (Thirlaway, 1966) and the discovery of the m_b - M_S discriminant, which works for similar sized explosions. The preliminary results of McLaughlin et al. (1983) on the Pearce processor provides some justification for re-examining complexity based on a physical interpretation of several observations of an event. Explosions recorded at distances from 15^o to 30^o also seem to be simpler, with fewer later arrivals in the P wave and smaller coda amplitudes, than earthquakes recorded at similar ranges and it may be worthwhile to examine ways to use this observation to discriminate smaller events.

A brief digression is useful to define some notation and introduce the major features of the upper mantle structure that seem to be world-wide. Figure 1 illustrates some typical travel time curves, appropriate for proposed models for northwestern Eurasia (Figure 2), and shows how the different branches will be referenced. If the structure under consideration contains a low velocity zone in the upper-most mantle, we will denote the P phase from the lithosphere (above the low velocity zone) as P_A. The model, K8, used to generate one of the travel time curves in Figure 1 has a deep low velocity zone and thus

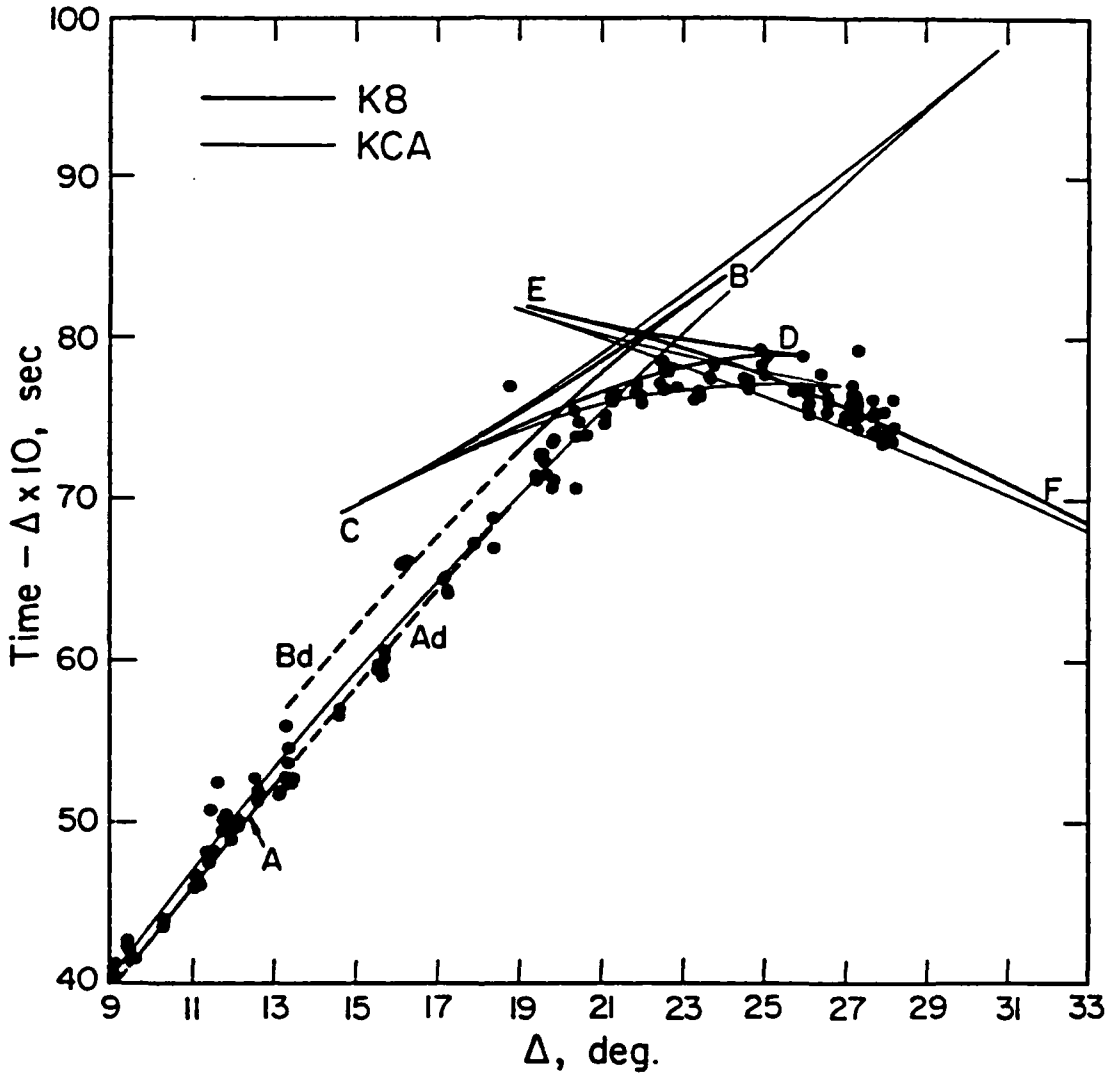

Figure 1. Travel time curves for two upper mantle models for northwest Eurasia. Observed travel times are from Novaya Zemlya events to northern European stations as reported to the ISC.

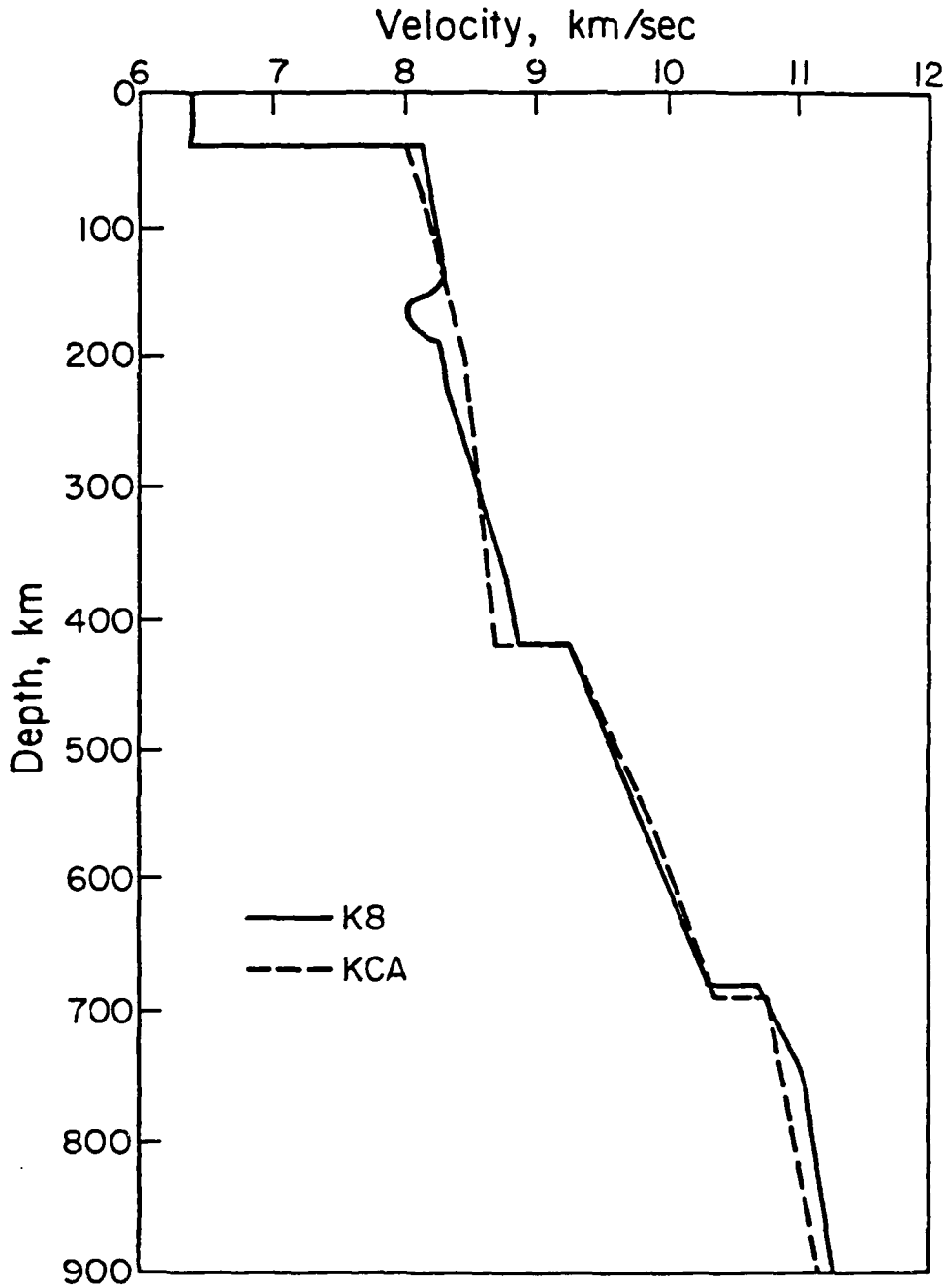

Figure 2. Two upper-mantle P-wave velocity models proposed for northwest Eurasia.

the P_A branch extends to near 12^o . In active tectonic regions of the world, the low velocity zone is hypothesized to be much shallower and P_A may only extend to 3^o P_A and P_n will be used interchangeably. P_B will refer to the P phase that bottoms below the low velocity zone and above the 400 km discontinuity; P_{AB}, then, refers to the AB branch of the triplication curves in the absence of a low velocity zone, consistent with the notation of most authors. P_{CD} refers to the P phase that bottoms between the 400 and 700 km discontinuity and P_{EF} refers to that phase from below the 700 km discontinuity. The retrograde branches P_{BC} and P_{DE} refer to reflections from the discontinuities. These branches are not separated enough in time from the forward branches, P_{AB} and P_{CD} to be distinctly observable phases and have been poorly constrained.

We show two P-wave models for northwest Eurasia in Figure 2. One, KCA, was derived by King and Calcagnile (1976) from apparent velocity data at the NORSAR array from presumed Soviet explosions. The Soviets have used nuclear explosions extensively in construction projects throughout western Russia and excellent data coverage of the main features of the travel time curve were available to King and Calcagnile (1976). Figure 3 shows the distribution of explosions and stations used in the study. Most of these source locations were used to derive KCA. Another model, K8, (Given and Helmberger, 1980) represents an attempt to reconcile the KCA model with waveform data

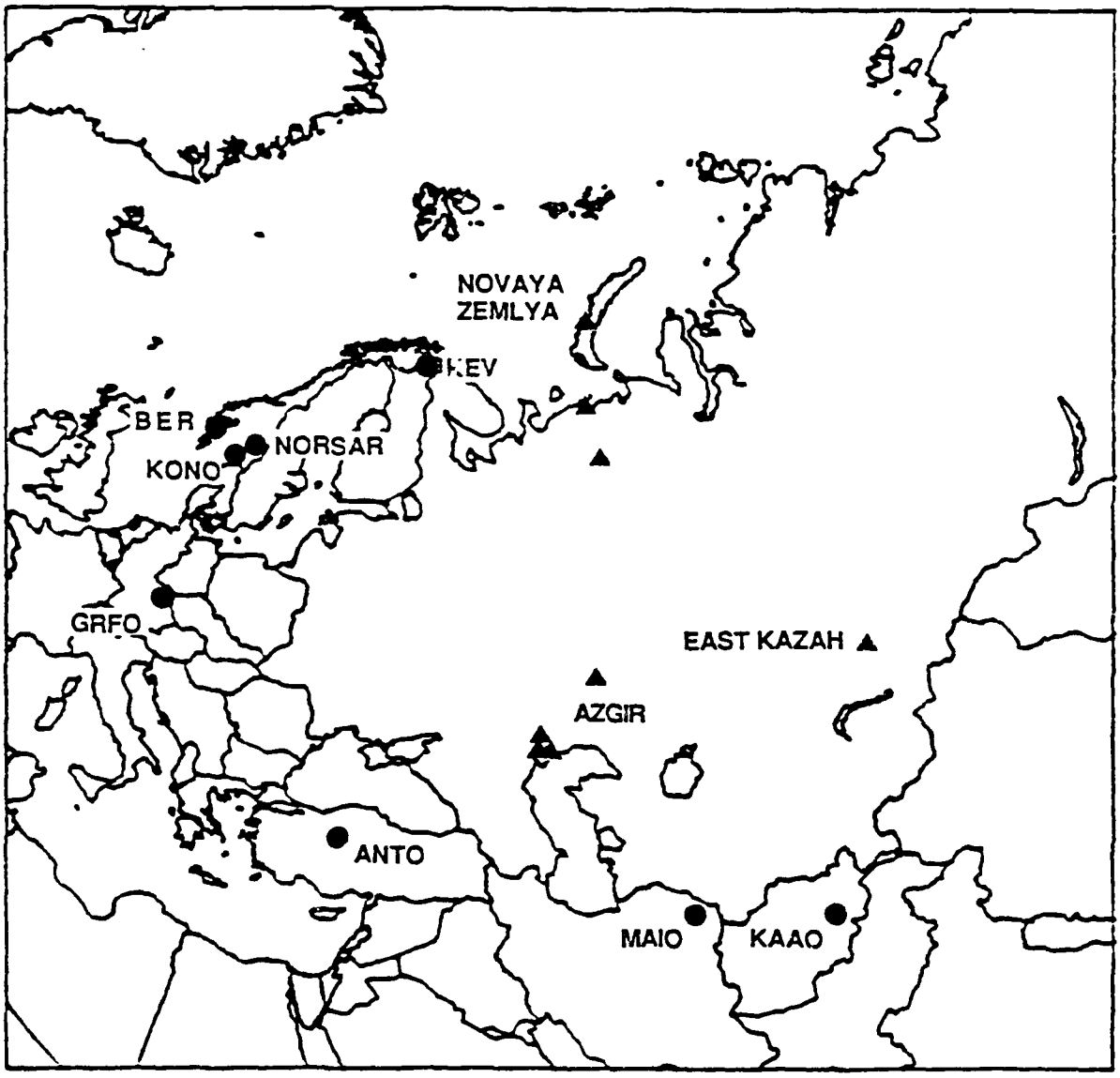

Figure 3. Location map showing station and event distribution for data discussed in this study.

observed on the long and short period WWSSN seismographs in Europe. These two models are most different above 400 km and particularly above 200 km. However, the travel times curves predicted by both are very similar, as shown in Figure 1, differing only in certain respects that are difficult to resolve. Although the models shown in Figure 2 appear very different, they only represent interpretations of different aspects of similar data sets. The available data can be simply characterized and appear consistent from event to event.

Figures 4 and 5 present synthetic record sections of K8 and KCA for comparison. The calculations were performed using a WKBJ method that does not accurately handle low velocity zones, however, the errors are not significant in view of the conclusions that we wish to draw. The differences between the two models in the synthetic calculations appear, at first, to be extensive, but they are actually not important in view of the substantial variation between individual observations. Each section reflects some attribute of the observed data that the authors incorporated into the velocity structure. KCA was derived to match the relative travel times measured on short period recordings as well as apparent velocity measurements and probably predicts more accurate travel times. However the relative travel times between the different branches are approximately the same for both models (to within 2 s for the poorly observed retrograde branch P_{BC}). K8 was derived to model observations of the relative amplitudes of the different P- wave branches over a wider region of Eurasia.

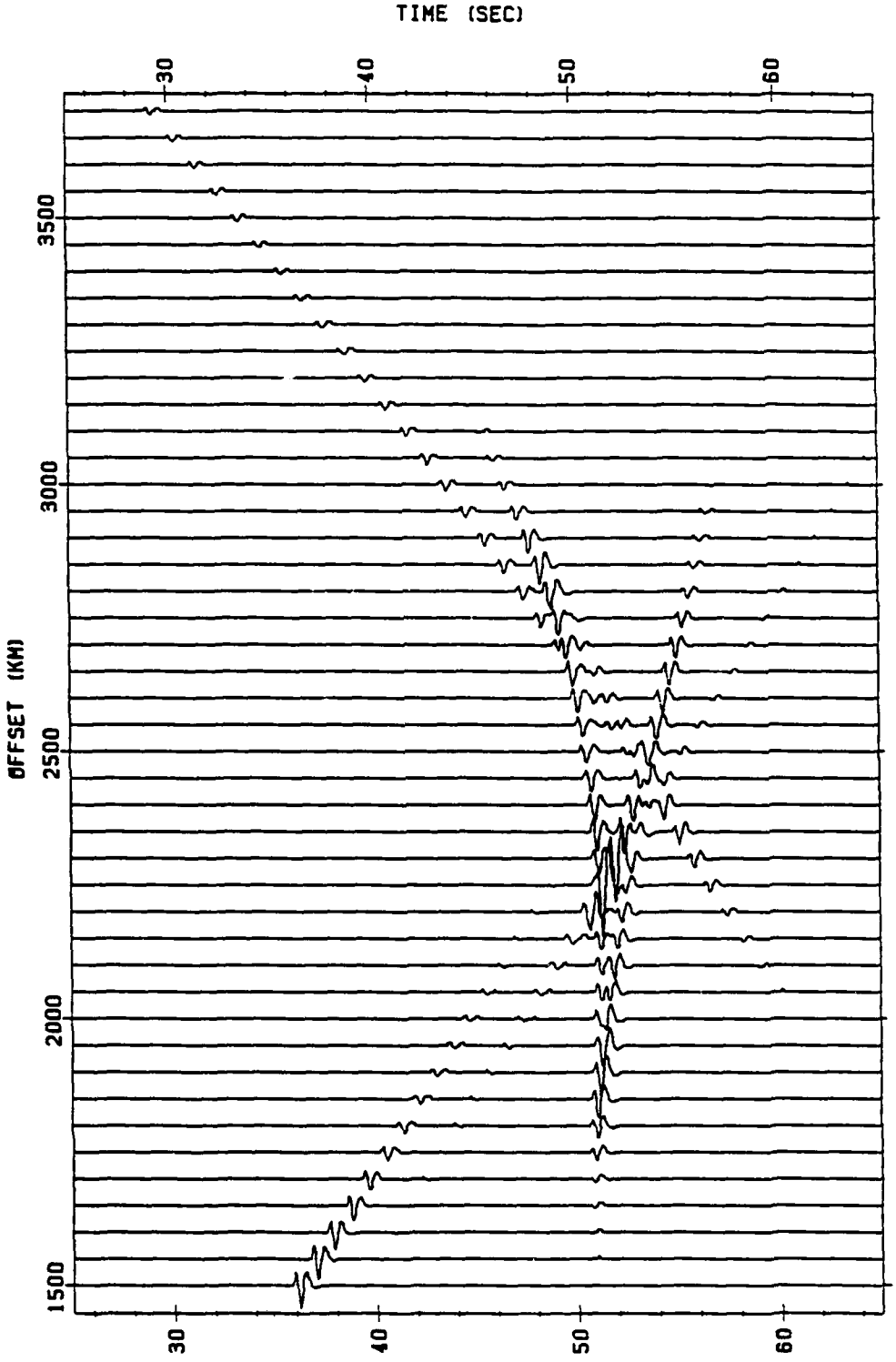

Figure 4. Synthetic seismogram profile for model K8.

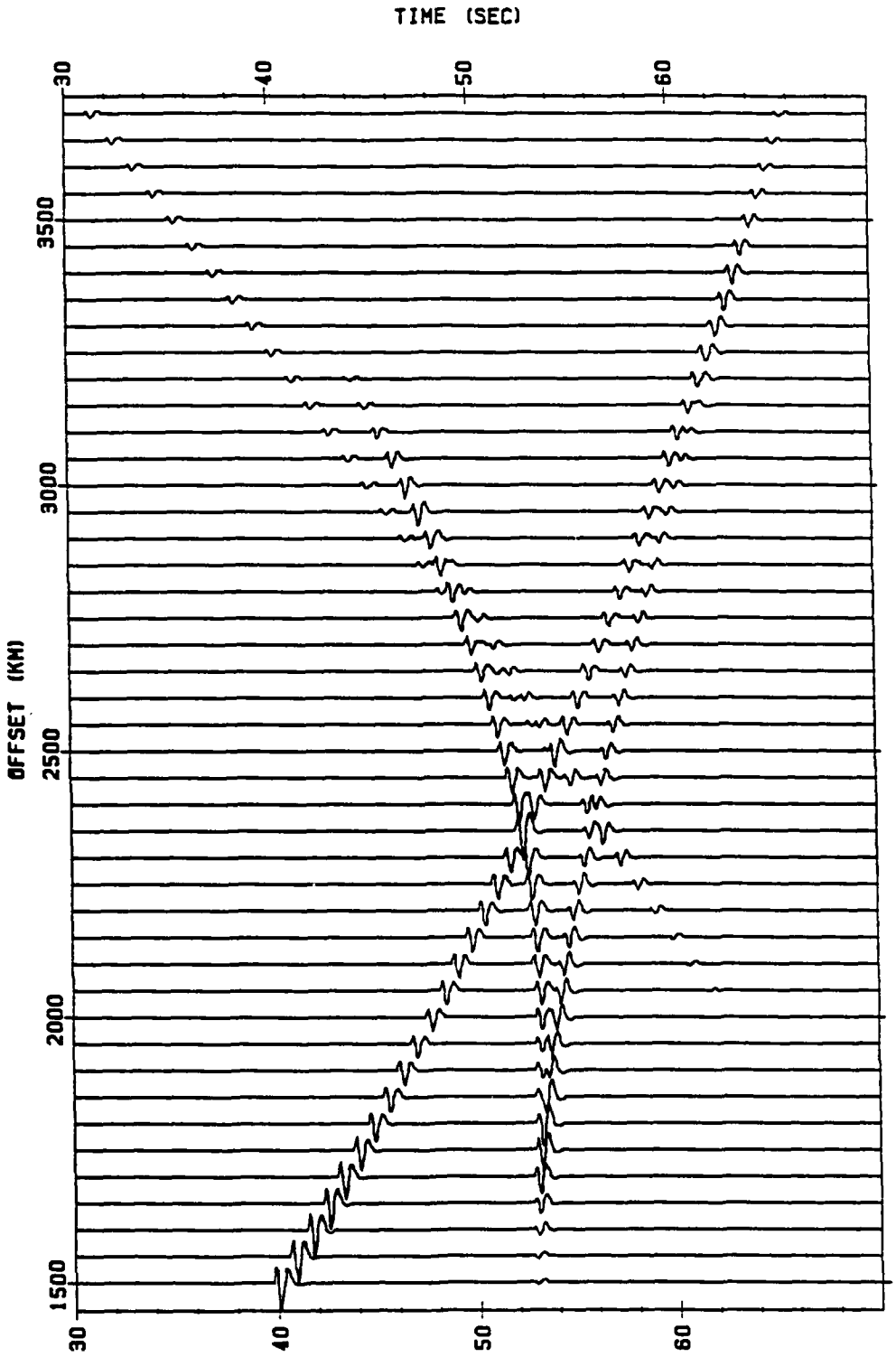

Figure 5. Synthetic seismogram profile for model KCA.

One observation, apparent in both Figures 4 and 5, is the amplification of the P wave arrivals from the upper mantle transition zone (400 to 700 km) relative to the P waves that have bottomed below 700 km. This is shown in the amplitudes of the P_{cd} branch relative to the P_{EF} branch, which are the first arriving P waves at distances beyond 2800 km. Thus we expect to see a factor of about three increase in the signal amplitude at distances between 1700 km and 2800 km over observations beyond 3000 km where most teleseismic analysis is performed. Of course the attenuation structure is an important consideration that has been largely ignored in Figures 4 and 5. These synthetics have been computed using a constant T^* (T/Q) assumption, implying an increase of Q with depth.

Based on our experience analyzing a large number of seismograms at these distances from northwest Eurasia, we can briefly summarize the general features of the seismograms recorded at upper mantle distances in northwest Eurasia. First, model KCA accurately reflects the relative travel times of the different branches. Second, the P_{AB} branch is an impulsive, distinct phase at the nearer distances (<1500 km), becomes attenuated and emergent between 1500 and 2200 km, again becomes a distinct phase between 2500 and 2800 km, and is intermittently observed between 2800 and 3500 km. The P_{CD} branch is a distinct phase between 1600 and 3000 km. Finally, the P_{EF} phase is not reliably observed before 2700 km, although it may appear as a later arrival near 2000 km. This phase is substantially weaker than

the P_{CD} branch and an abrupt amplitude decay of a factor of three is anticipated beyond 3000 km. Of course, since we are discussing short period seismograms, the observations vary enormously. In the following, we present examples of the data to illustrate our characterization of the upper mantle P-wave propagation.

3.1 Observed P Waves From 700 to 1500 km in Northwest Eurasia

The important observations at distances between 700 and 1300 km are that the P-waves at periods greater then 2 s are simple and impulsive. This observation was documented on the long period WWSSN seismograms in Given and Helmberger (1980). Examples of short-period seismograms at these distances are shown in Figures 6 and 7. The P phases are complex at the high frequencies, with an energetic, high frequency coda. At distances beyond 1000 km, it appears that the high frequencies lag the first arrival by several seconds as shown in Figure 8, which is a filtered version of Figure 7. Even so, at the shorter periods, the seismograms at these distances show impulsive and distinct P waves. Furthermore many of the explosions from the western Soviet Union generate large amplitude, distinct Sn phases (see Figures 6 through 8). Both the direct P and S phases in Eurasia travel at apparent velocities that are among the highest observed worldwide for these phases at these distances. The observations imply that the upper 100-150 km of the mantle in this region has both high velocity and low attenuation.

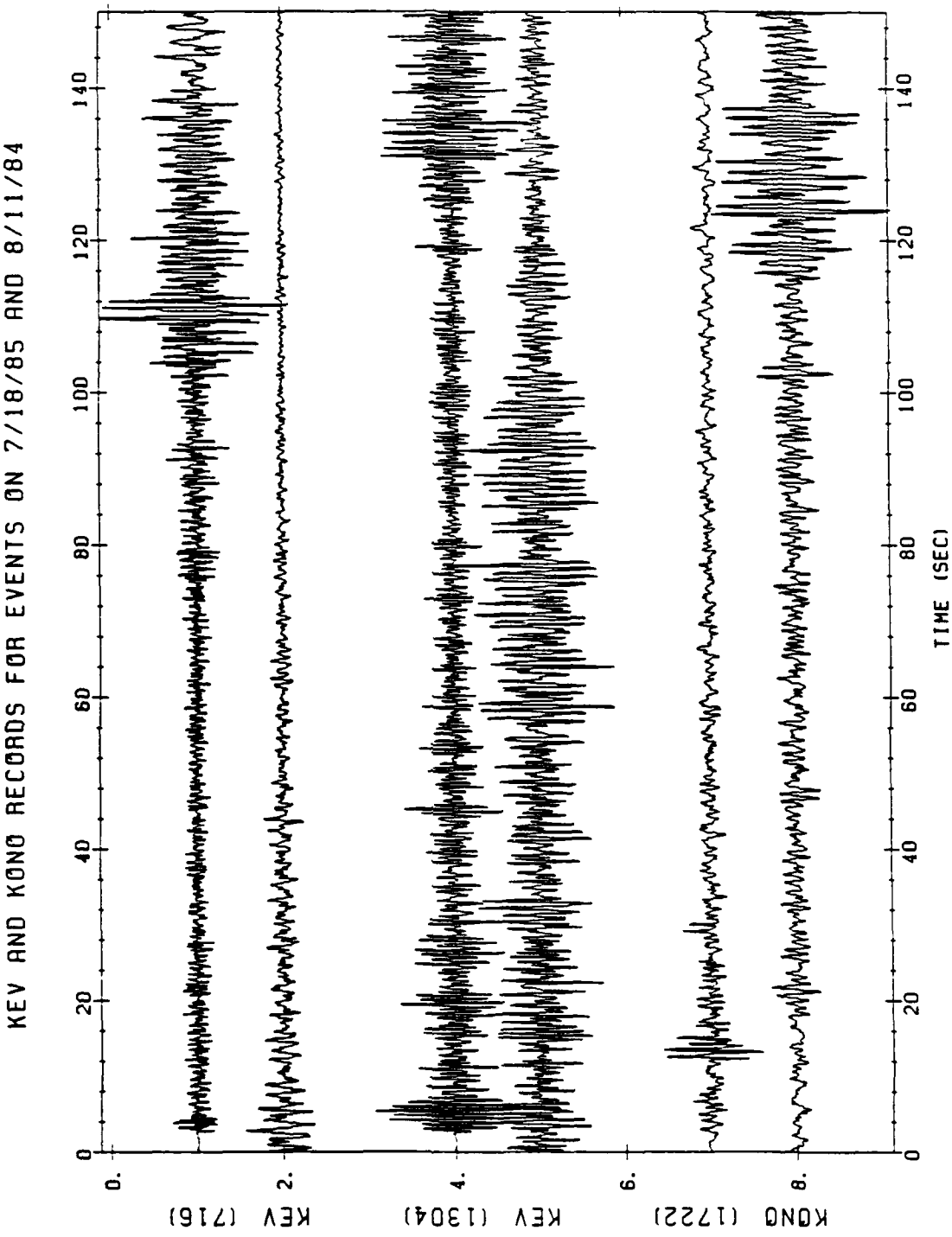

Figure 6. Observed seismograms from Soviet Peaceful Nuclear Explosions. Each record is a continuous seismogram 300 s long. The top and bottom traces are from event on 21:14:57, 18 July 1985; the middle trace is for event on 18:59:57, 11 August 1984.

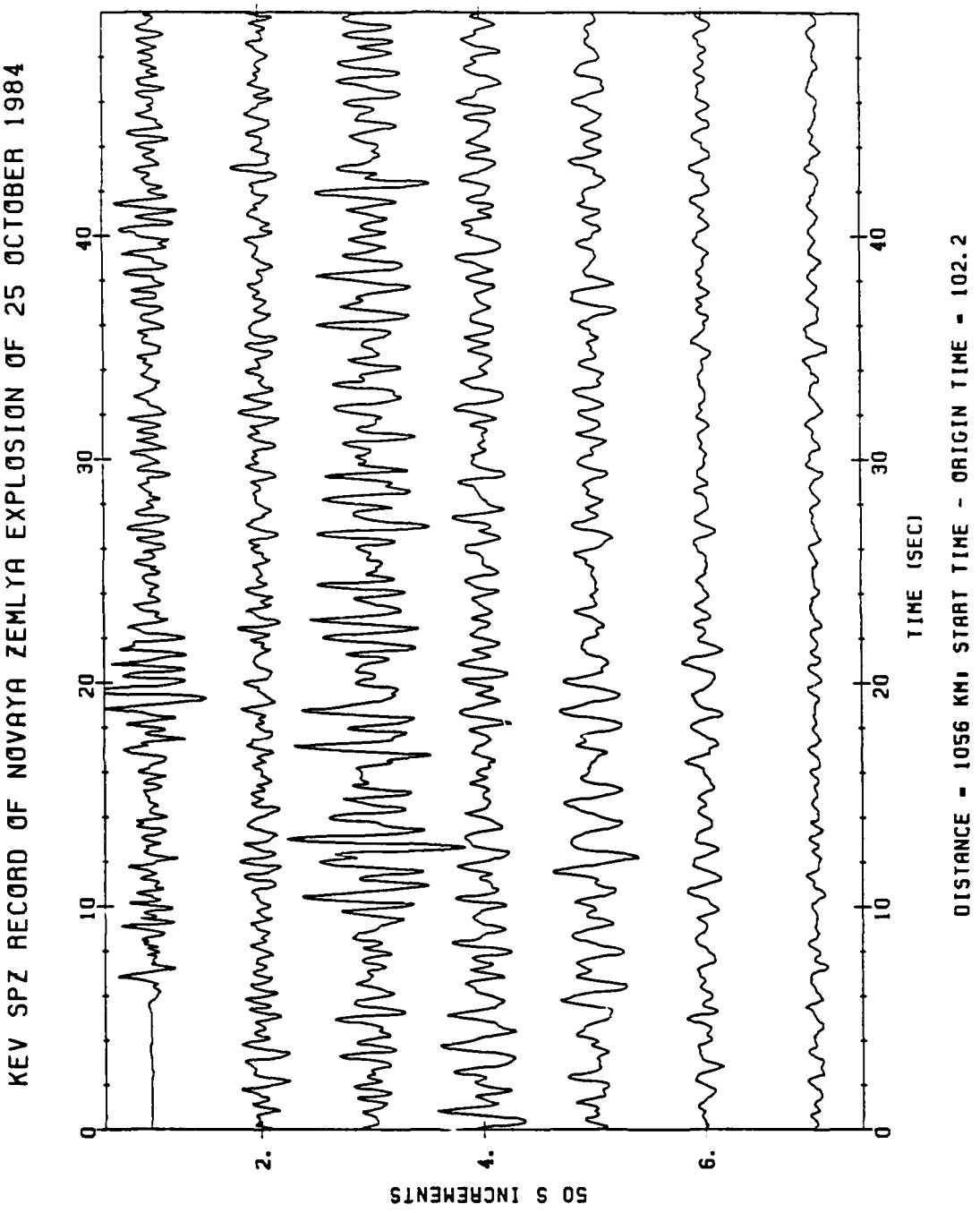

Figure 7. Observed short-period vertical seismogram at DWWSSN station KEV from Novaya Zemlya explosion. A continuous seismogram, 350 s long is shown. Initial P wave is impulsive; strong later phase at 12 s, which may correspond to PP. Distinct S_n phase at 110 s.

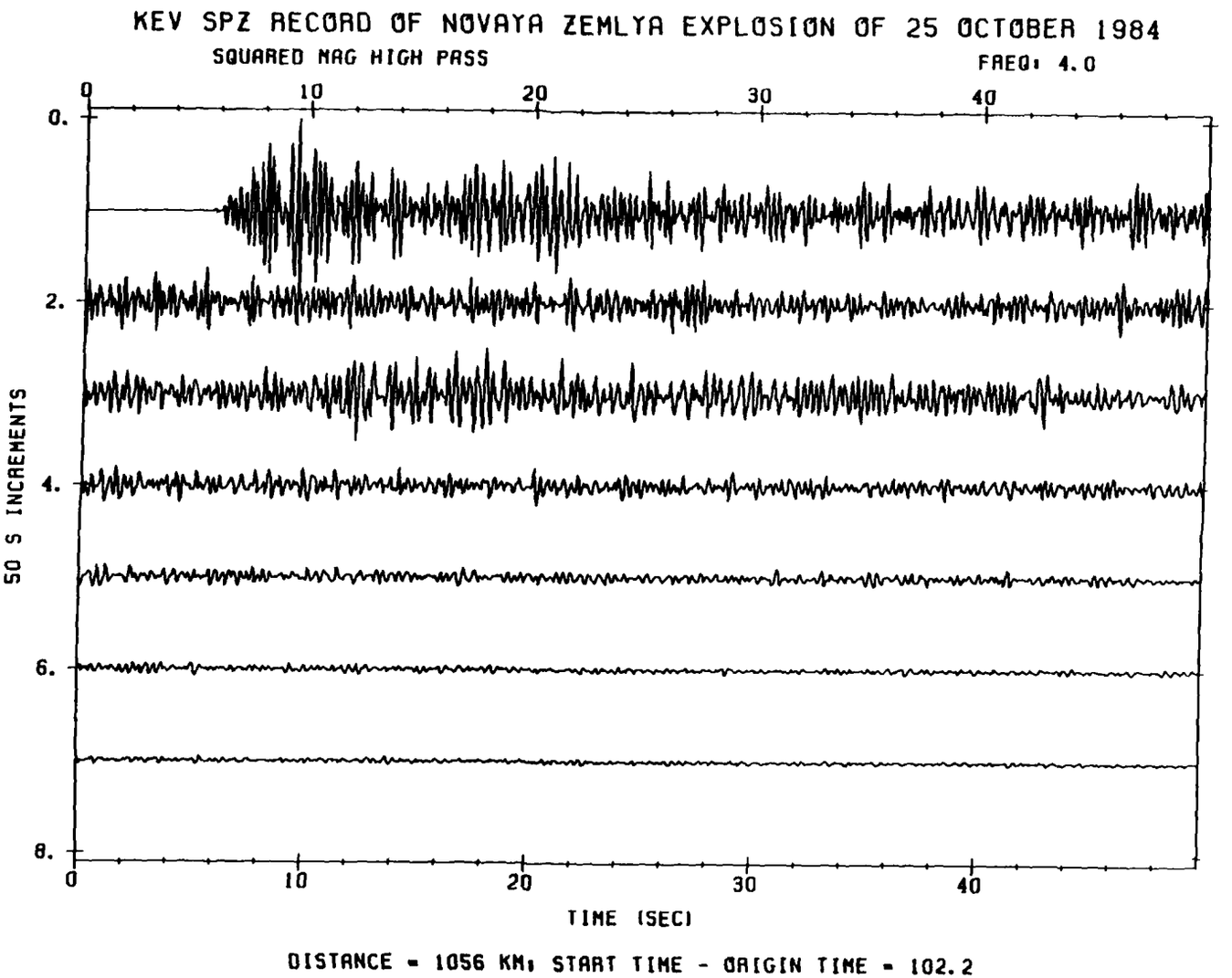

Figure 8. Same seismogram as shown in Figure 7 except filtered with high pass filter at 4 Hz. The high freqencies are emergent and are delayed from the first arrival by approximately 2 s; S_n is barely visible above the coda.

Velocity structures such as KCA or K8, with weak, positive velocity gradients in the upper mantle will give rise to large amplitude, impulsive P_A (P_n) phases to distances beyond 1000 km. This is in contrast to the low amplitude emergent P_n phases that are observed in active tectonic regions such as the western U. S. Furthermore, a well defined P_g phase that is often present in regional seismograms recorded in the western U. S. is absent in the stable continental regions of Eurasia. The low amplitude of the initial P wave has been the basis for including a low velocity zone in proposed models for the uppermost mantle in the western North America. Langston (1982) has calculated theoretical seismograms for some simple uppermost mantle models and has shown that the amplitude of the initial P wave is very sensitive to the velocity gradient in the uppermost mantle. He shows that the general behavior of the regional P-phases (both P_n and P_g) in the western U. S. can be explained qualitatively by a simple layer over a half space velocity model. Observations of large amplitude P_n phases and relatively small P_g phases, such as are common in Eurasia and the eastern U.S. require a model with a positive velocity gradient in the uppermost mantle. Of course, the attenuation structure is playing an important role in the amplitudes of the regional waveforms and it is difficult to separate the effects of Q from the velocity structure. Certainly, the western U.S. is more attenuating than the more stable continental regions of the world (Der et al., 1986).

The thick continental lithosphere, implied by the high P-wave velocities and low attenuation in the uppermost 150 km in western Eurasia, has implications for discrimination. The models KCA and K8 predict that, at distances less than 1200 km, the P_n phase is a direct phase from the source region while P_n in western North America is a diffracted phase (similar to a head wave) with much of the high-frequency source information distorted by propagation effects as well as attenuation. These differences imply that much smaller events are observable at these ranges in regions such as northwest Eurasia. Langston (1982) has shown that similar structural differences between the eastern and western U.S. can account for the m_b bias of up to a full magnitude unit between the eastern and western U. S. found by Evernden (1967). Furthermore, these models suggest that S_n (or in our notation S_A) should be a dominant phase in the stable continental regions and should be difficult to observe in the tectonic regions. Short period S-waves, with arrival times appropriate for phases that have propagated through the upper mantle, are commonly observed in both northwest Eurasia and eastern North America from both earthquakes and explosions. Some examples from Eurasia are shown in Figures 6 and 7. S_n, where it is observed, should similarly carry information about the source and, used in conjunction with P_n, may prove to be a useful discrimination tool.

The complex, high frequency P_A phase continues to near 1500 km; the available P-wave data has a strong coda that persists for 20 s

duration. An example is shown in Figures 9 through 11, a NORESS recording of a Soviet PNE at 14^{o}. The delay of the high frequencies relative to the first arrival is even more striking in this example, suggesting that the velocity structure, or the attenuation structure, is reducing the amplitude of the first arrival relative to the coda, which can propagate as scattered energy in the high Q, high velocity uppermost part of the mantle. The low amplitude character of the first arrival persists to at least 20^{o}, the distance where P_a ceases to be a first arrival. An interesting observation is the presence of very small precursors to the P waves to distances beyond 20^{o}. This is documented in Given and Helmberger (1980) and in Figure 12 in a NORESS recording of a Novaya Zemlya explosion. This feature is what is expected if the first arrivals are scattered or diffracted waves travelling in the lithosphere while direct arrivals are shadowed by either pronounced low Q or a low velocity zone, such as was included in model K8. It also implies that, in many cases, polarity information based on first motion estimates may be unreliable at these distance ranges.

3.2 P-Wave Seismograms Between 1600 and 4000 km in Northwest Eurasia

A representative section of explosion data from Eurasia is displayed in Figure 13. These data were selected to cover a diversity of travel paths (East Kazakh to Fennoscandia), include a variety of instruments (DWWSSN, NORSAR, SRO, ASRO), and be representative of the variation in

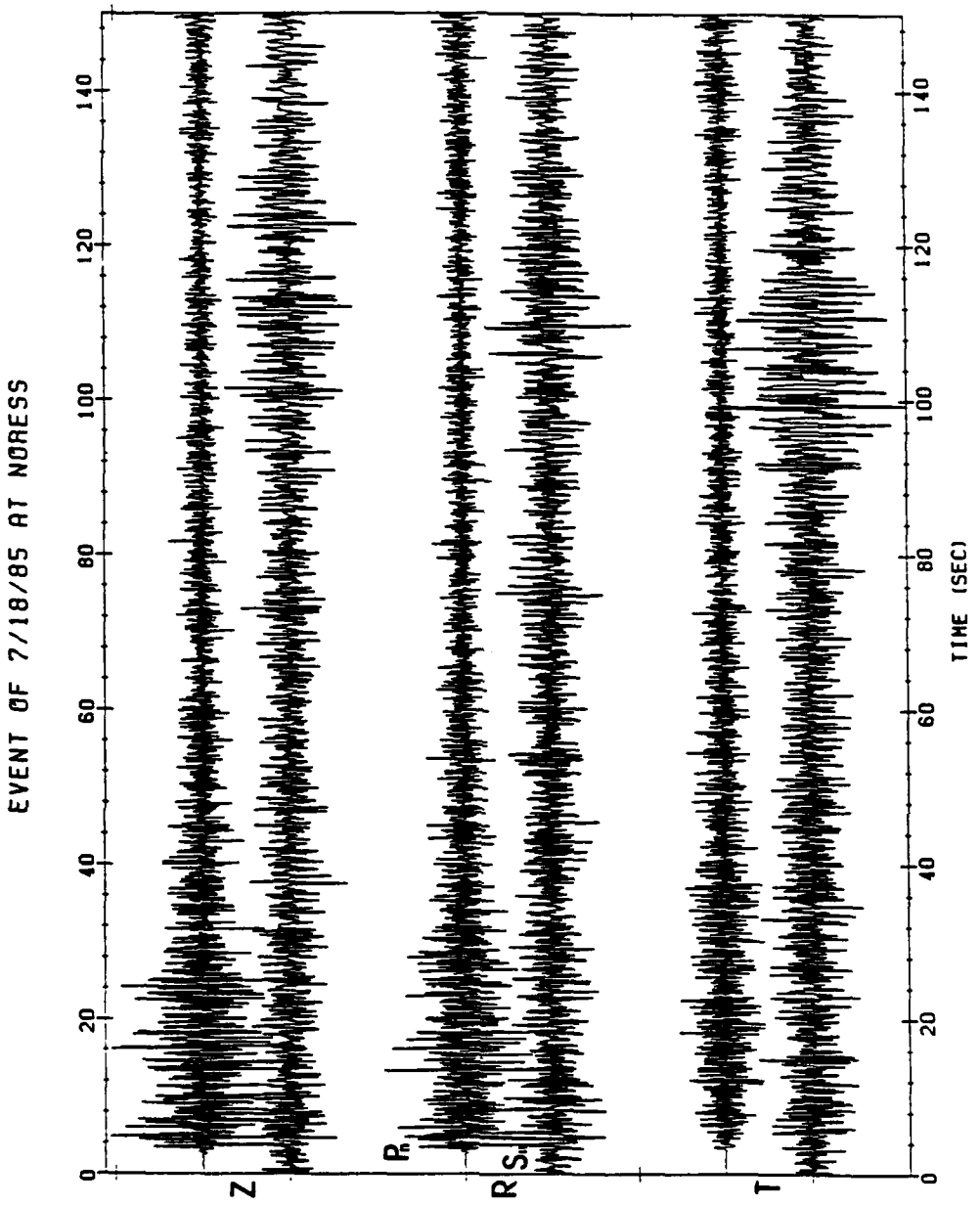

Figure 9. NORESS (NRAO) seismogram of Soviet explosion (PNE on 18 July 1985). P_n and S_n phases are indicated. Each pair of traces is a continuous seismogram 300 s in duration.

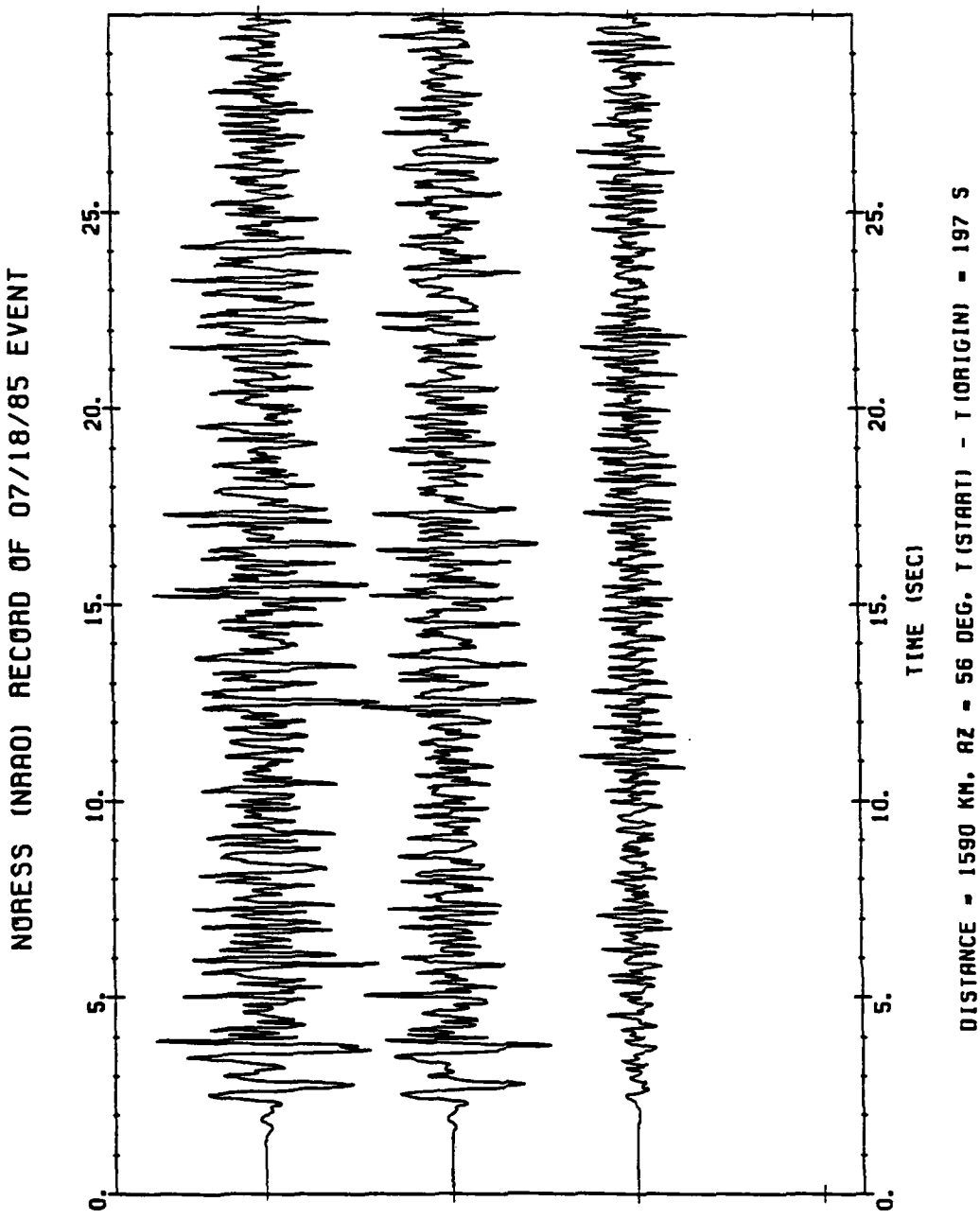

Figure 10. First 30 s of 3 component NORESS seismograms shown in Figure 9. Top trace is the Z component, the middle and bottom traces are the radial and tangential components. Note that P_n is slightly emergent and that the high frequences are delayed from the first arrival by over 2 seconds.

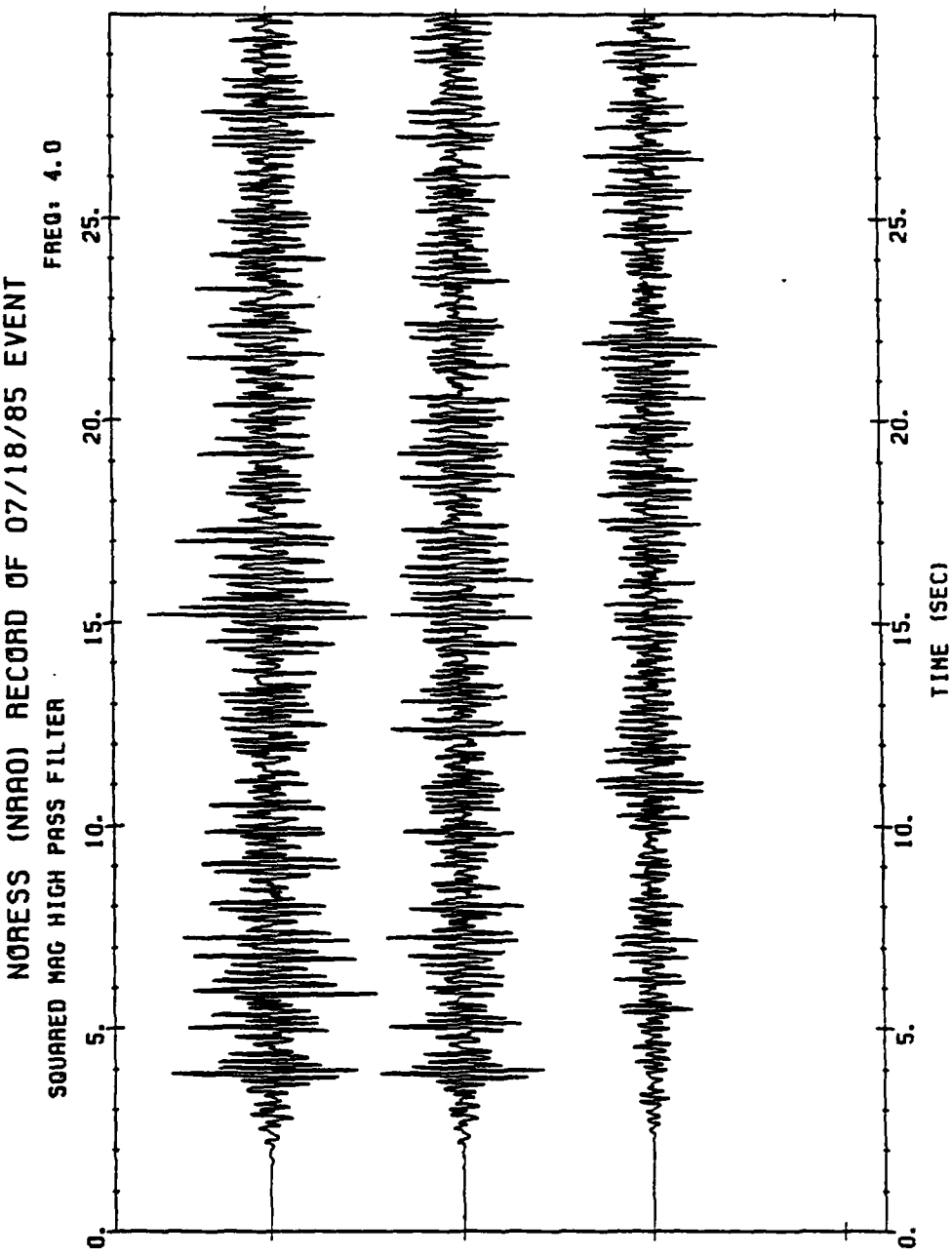

Figure 11. NORESS seismogram from Figure 10 filtered at 4 Hz. The components are vertical, radial and tangential from top to bottom.

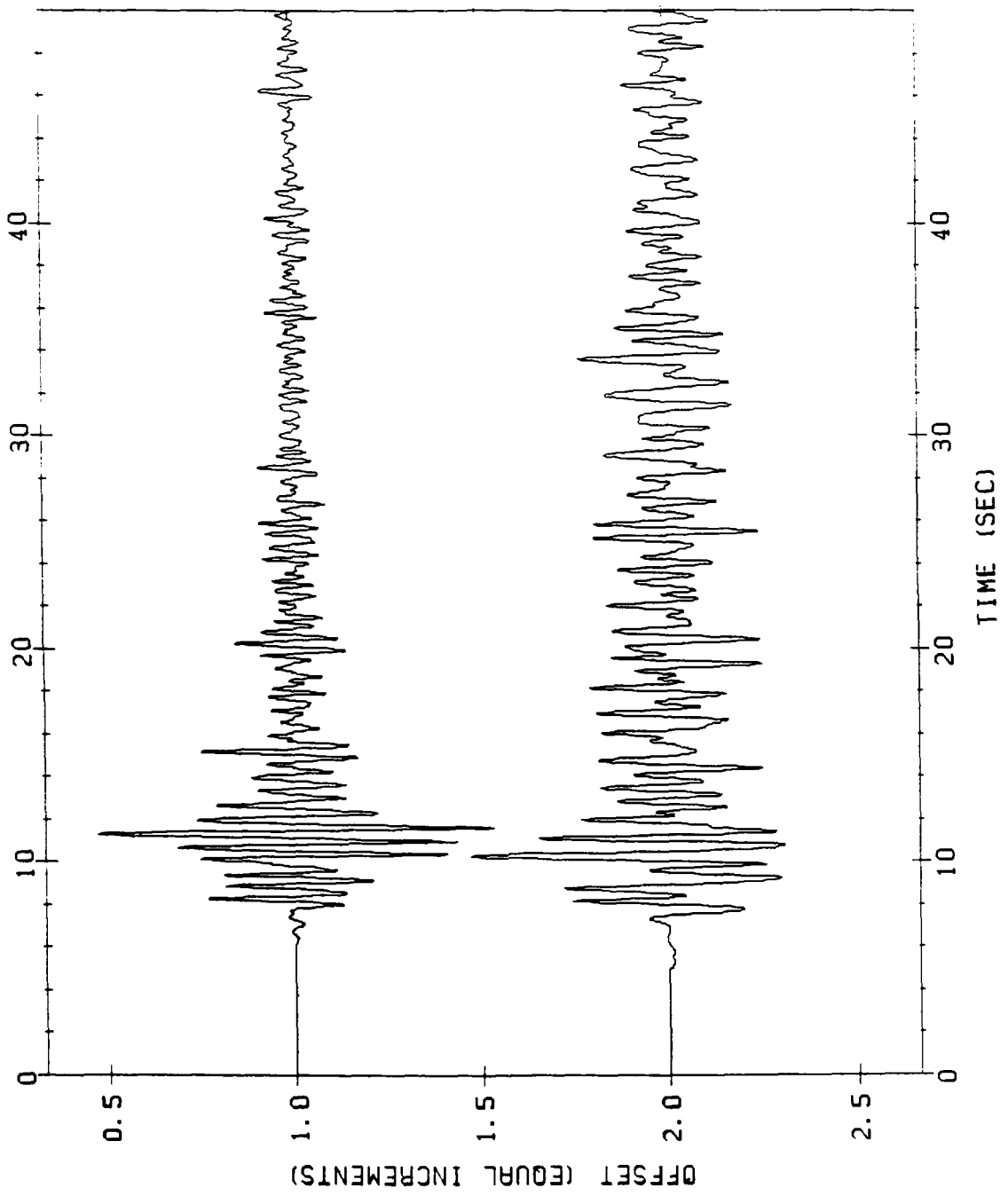

Figure 12. Seismograms from Novaya Zemlya explosion of 25 October 1984, recorded at NORESS (top, array sum) and KONO (bottom). Distance to NORESS is 2275 km; distance to KONO is 2430 km. The NORESS P-wave has a small precursor 2 s before dominant arrival. At KONO this arrival is either not present or obscured by poor signal to noise. Record starts at 0 s for the NORESS seismogram and at 5 s for the KONO seismogram.

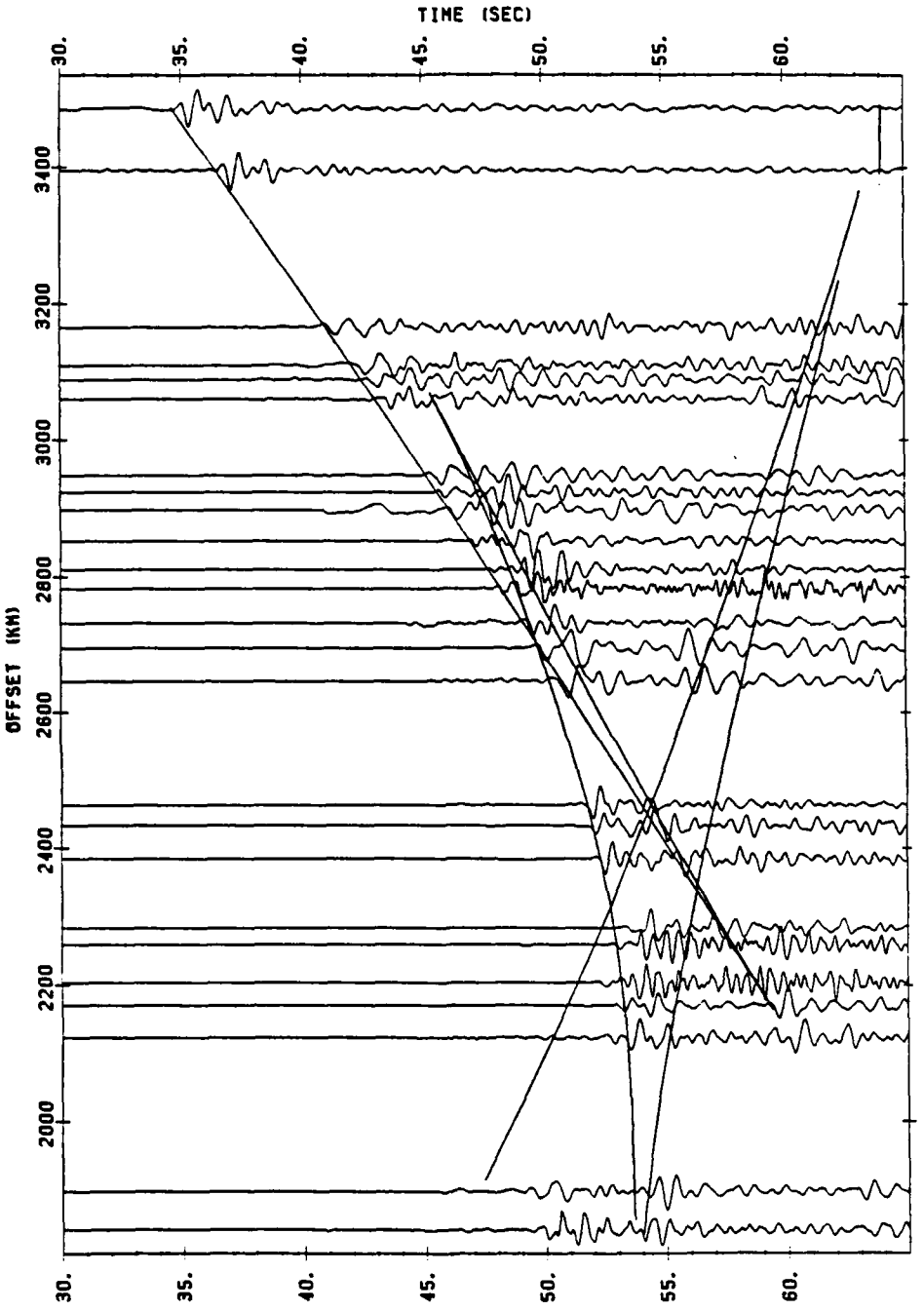

Figure 13. Sample of explosion data from Soviet test and PNE's. Data is intended to show variation in upper-mantle observations and are from a wide region including northwestern Eurasia and central Asia. Superposed travel time curve is for model KCA.

complexity typically observed in upper mantle seismograms. This figure shows that, in general, a large part of the complexity observed can be attributed to the velocity structure. Arrivals predicted by model KCA can usually be imagined to be present in the data. However, given this data set, it would have been difficult to conclude anything about wave propagation in the upper mantle, which points to the importance of array studies, such as that of King and Calcagnile (1976), to isolate the important phenomena.

The data shown in this section is not presented with the idea of proving or disproving a particular velocity structure but to demonstrate the variability and predictability of these seismograms. We have sought to obtain data from as many explosions from Eurasia as are available. It is of interest to note that the variation between the seismograms in Figure 13 and the synthetics in Figures 4 and 5 are less than the variations often observed between individual stations in the NORSAR array recordings in Figure 14. This is remarkable considering that the data in Figure 13 comes from a wide geographical region and includes many different source - receiver pairs.

Near 1600 km, a strong, discrete phase appears 10 s after the initial P arrival (see, for example the KONO seismogram in Figure 6). This phase is the P_{CD} phase and in Eurasia is a pronounced phase until beyond 2900 km. It becomes the first arrival near 21^{o}. Both KCA and K8 predict the onset of this phase at 1600 km and its and disappearance at 2900 km, although the relative arrival times with respect

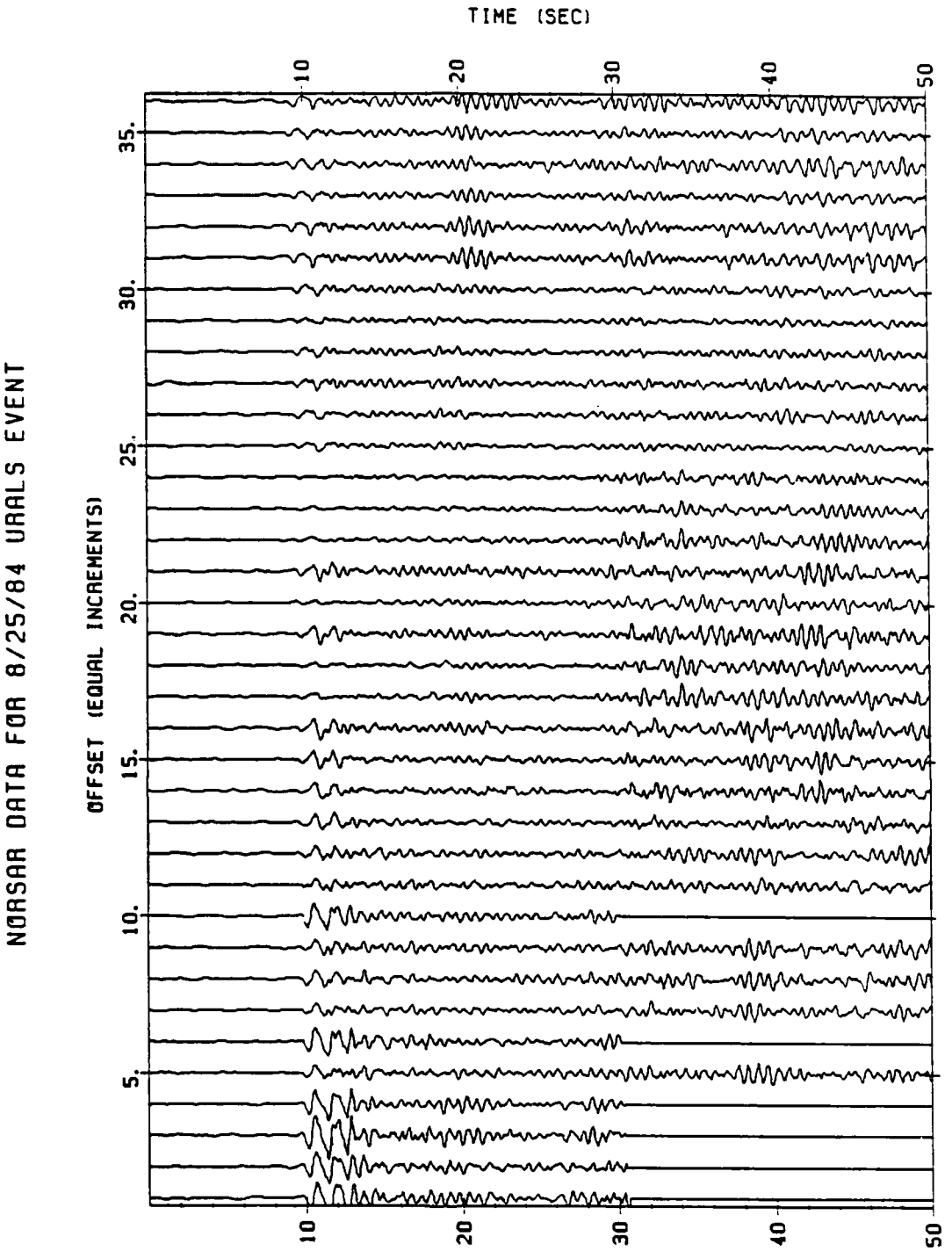

Figure 14. NORSAR array seismograms for Soviet PNE at 3160 km (to N1A0), 61° azimuth. Seismograms are arranged in increasing distance. There is a large variation in the relative amplitudes of the inital P arrival and the coda. The initial P arrival is P_{EF}; the P_{AB} branch is expected near 30 s and appears as a diffuse arrival with an extended coda.

to the other branches differ by up to 2 s. (These differences appear in the back branches, P_{BC} and P_{DE}, which are difficult to observe.) The variation in the relative travel times is of the same order as the regional variation in the observations. The P_{CD} phase has a large amplitude due to the strong positive velocity gradient between 400 and 700 km. In the observations presented in King and Calcagnile (1976), it is consistently observed. There is some evidence (Grand and Helmberger, 1983, 1984, Rial et al. 1984) that the upper mantle below 400 km is much less heterogeneous than it is above 400 km. Given the reliability of observing this phase in northwest Eurasia, it may be a more useful phase for locating and analyzing events in the distance range of 1500 to 2000 km.

The largest differences between the two models, K8 and KCA, is in the predictions for the P_B (or P_{AB}) branch. Model K8 can predict the amplitude behavior of the P_{AB} and P_{CD} phases between 15 and 20^o using an attenuation structure that increases with depth such that T^* (T / Q) is constant; KCA requires additional structure in either velocity or attenuation. Der et al. (1985) have investigated the attenuation structure of the upper mantle using essentially the same data set as King and Calcagnile (1976) by comparing the spectra of the different branches. Their attenuation model for Eurasia predicts T^* differences

($T^*(P_{AB})$ - $T^*(P_{CD})$) of 0.1 to 0.05 between 1600 and 2200 km, which will probably help explain the observed relative amplitudes, but more modeling work is required to confirm this.

In general, beyond about 1600 km, the amplitude of the first arrival, the P_A phase diminishes relative to the P-wave coda and the arrival from below the 400 km discontinuity (P_{CD}). At distances beyond 2400 km, the P_B branch becomes a discrete observable arrival as seen in the King and Calcagnile (1976) data. Between 1600 and 2400 km, there is considerable complexity and variability associated with this branch. Beyond 2700 km the P_{AB} branch again develops an extended coda. In some NORSAR data, the P_{AB} branch, with its extended coda, is observable to 3500 km. Examples of the data constraining the P_{AB} branch are shown in Figures 14 and 15. KCA was derived to fit these observations. On the other hand, K8 was constrained to fit the observation that no long period seismograms from Europe show any evidence of the P_{AB} branch beyond 24^o and that the P_{AB} branch on short period seismograms is often not visible as a discrete arrival. This discrepancy can be qualitatively resolved by invoking lateral heterogeneity. King and Calcagnile (1976) describe how heterogeneity above the 400 km discontinuity can prolong the branch several degrees. Also, if the Q in the lithosphere is high enough relative to the rest of the upper mantle, high frequency energy propagating as scattered energy in the upper 100 km will arrive at times appropriate to extend

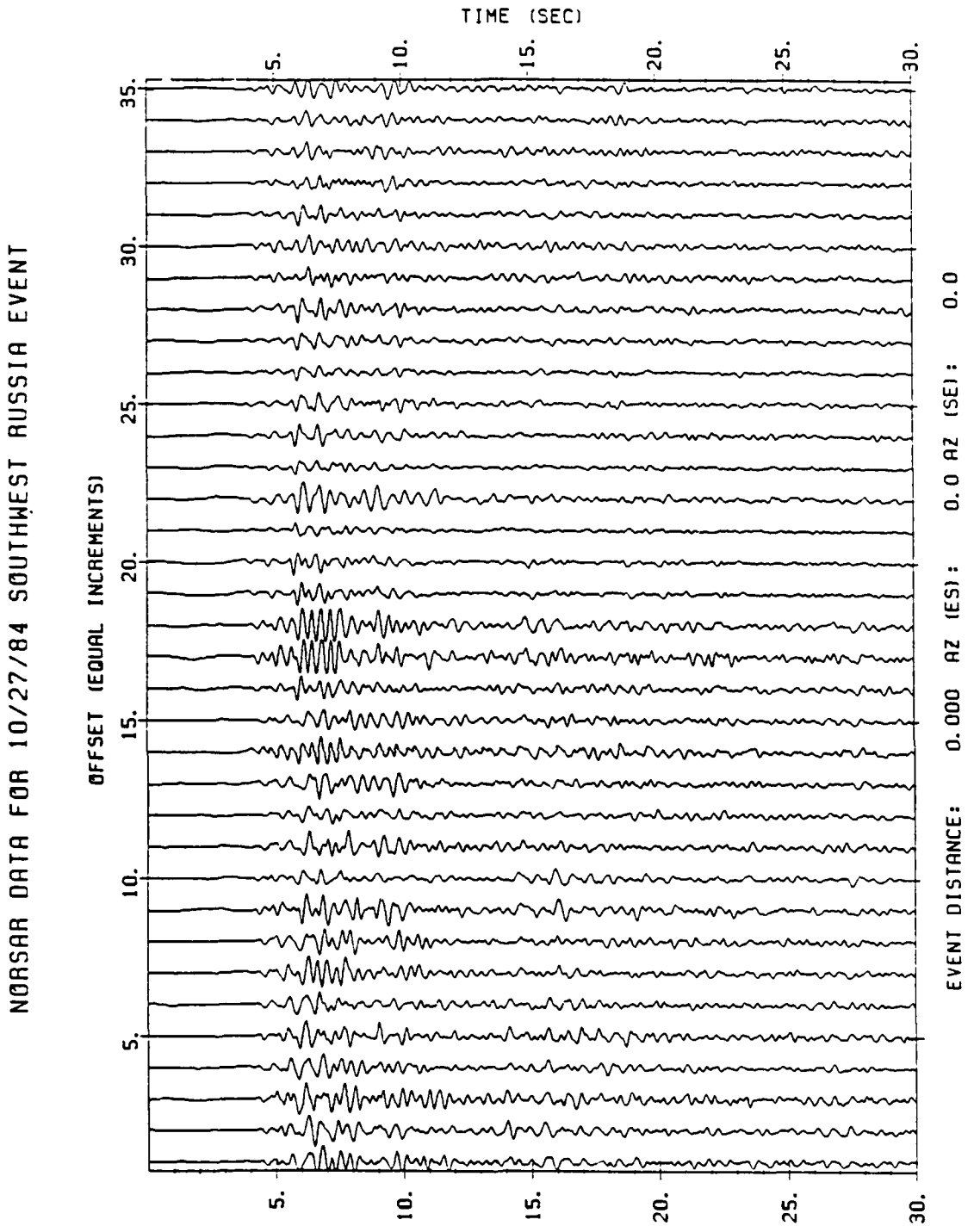

Figure 15. NORSAR array seismograms for Soviet PNE at 2884 km (to N1A0), 106° azimuth. The dominant arrival is P_{CD}, which arrives 1 - 2 s behind the initial P arrival (P_{EF}). The expected time for the P_{AB} phase is expected nearer 15 s and is not an obvious arrival.

the coda. For our purposes it is sufficient to observe that energy associated with the arrival time of the P_{AB} branch of KCA cannot be reliably used to estimate source parameters.

At 19°, the P_{EF} phase appears although it is often difficult to observe since it arrives in the coda of the usually larger P_{CD} phase. At this distance it is better observed in other parts of the world such as in the data presented by Walck (1984) for the Gulf of California. It also appears to be a distinct phase on some of the records in Figure 13 at distances near 2000 km. These seismograms are from central Asia (East Kazakh to MAIO) where the upper mantle may be significantly different, yet model KCA still predicts the relative arrival times of the primary arrival. Between 19° and 24° it is often difficult to isolate the P_{EF} phase, probably because it is smaller in amplitude relative to the earlier arrivals. P_{EF} becomes the first arrival near 24.5 ° and beyond that distance it is roughly 1/3 the amplitude of the P_{CD} phase.

We have tried to present examples to illustrate that, as general conclusions concerning the velocity structure in Eurasia, it appears that energy associated with the P_{CD} and P_{EF} branches is consistent over large regions and may be confidently modeled. Energy associated

with the P_{AB} branch, particularly from the uppermost 200 km is highly variable and represents a significant source of noise from a modeling point of view.

3.3 Modeling Considerations Using Upper Mantle Seismograms

We ultimately wish to use this data to constrain focal mechanism and depth through deterministic modeling of observed events, and therefore, it is important to evaluate the potential performance of any method that relies on recognizing discrete depth phases. A rough way to make this assessment is to examine the complexity in the first 20 - 30 s with attention to how reliably the arrivals of the various P-phases are predicted and how much additional unmodeled energy is present. Additional arrivals may be associated with depth phases and can be used to test potential focal mechanisms. Furthermore the coda the of the P-wave, or the amplitude level outside the windows of expected arrivals, can be used to constrain possible focal mechanisms as in the implementation of the Pearce algorithm described in McLaughlin et al. (1983, 1985)

From Figure 12 it appears that coda levels are typically smaller than the amplitude of the predicted upper mantle arrivals, an observation that may be useful in the application of a Pearce algorithm using such data. Even so, there is a significant amount of unmodeled noise that will make constraining the amplitude of depth phases difficult. Additional processing, such as array beaming or polarization

filtering, will clean up the data somewhat, but the enhancement is no better than that observed at teleseismic distances. Each of the upper mantle arrivals will have a coda associated with it (the retrograde branches will even have a "coda" preceeding it). However, while the upper mantle arrivals seldom interfere constructively, the respective codas always add constructively, and, thus, noise levels and perceived complexity will be greater at these distances.

McLaughlin et al. (1983) showed that, if the coda amplitudes do not exceed the P phase amplitudes at 4 stations with good azimuthal coverage, then assigning relative amplitudes of pP and sP to P based on the coda amplitude is sufficient to (theoretically) rule out all double-couple mechanisms. The McLaughlin et al. (1983) study dealt with observations at teleseismic distances appropriate for observing takeoff angles of around 20°. At upper mantle distances, the takeoff angles are larger and this conclusion needs to be re-evaluated. This is done in the next section. A more difficult problem is the detection of multiple explosions and the discrimination between these events and earthquakes at depth. We will examine the difficulties encountered in modeling short period seismograms from shallow events at regional distances in a later section.

4.0 Synthetic Tests on Extending the Pearce Processor to Upper-Mantle Distances

Most of the work on developing techniques, like the Pearce algorithm (Pearce, 1977, 1979, 1980), has been on analyzing data from events recorded at teleseismic distances. Seismic energy from small events is often reduced to the noise level by the time it has travelled these distances. As we have seen, seismograms from 10 to 25°, show (at least theoretically) an amplification in the signal level of as much as a factor of three due both to the closer range and to the large velocity gradients in the upper mantle.

Careful consideration is required to determine if a discrimination technique developed at teleseismic distances can be reliably extended to upper mantle distances. One of the important factors in extending the Pearce algorithm to the nearer ranges is that the energy arriving at those distances has come from a different part of the focal sphere, with higher angles of incidence than encountered at teleseismic distances. Another factor is that one arrival can be replicated into as many as 5 distinct arrivals by passage through the upper mantle structure. To examine the effects of these differences, a series of experiments using synthetic data in the Pearce algorithm were conducted.

The Pearce algorithm involves iterating through a set of possible focal mechanisms and determining whether or not the amplitude ratios,

pP/P, sP/P, and sp/pP theoretically predicted for each mechanism are consistent with the measured amplitude ratios. The set of mechanisms used in this series of experiments can be represented by a grid with sample points every 10^{o} in slip, every 10^{o} in dip, and every 30^{o} in strike, giving a total of 3888 possible mechanisms. Part of the power of the algorithm is that the measured amplitudes do not need to be specified exactly, instead each amplitude is described by a maximum and minimum possible value. Following this idea, the synthetic data used in these experiments were chosen to have both a maximum and minimum P amplitude of 1 and pP and sP amplitudes that range between 0 and 1. Polarity was not considered and, in some cases, the sP information was ignored. These experiments were designed to be similar to the ones performed in McLaughlin, et al. (1983) in order to extend their results to nearer ranges.

The typical complexity observed in the upper mantle seismograms from explosions, such as those presented in Figure 13, is such that the coda amplitudes seldom exceed the maximum amplitude of the upper mantle arrivals. We want to examine whether this level of complexity is enough to eliminate the possibility that the event is an earthquake and what the required station distribution must be. Further observational work on seismograms from explosions will be necessary to thoroughly characterize the range of expected complexity in these seismograms.

Effects resulting from changes in takeoff angle were first examined for a single station. For each of 8 takeoff angles ranging from 10 to 45°, the Pearce algorithm was applied and the percentage of consistent focal mechanisms was computed. The results are plotted in Figure 16. Also indicated in the figure are the results determined by McLaughlin et al. (1983) when they use both pP and sP information. Their pP only values are almost identical, differing by less than 2 percent, which suggests that sP provides very little additional information. The triangles represent our values using only pP information, while the circles show our values when sP is included. Our pP only results agree quite well with McLaughlin et al.'s (1983) and indicate that fewer focal mechanisms can be eliminated as higher takeoff angles, corresponding to closer distances, are reached. When the sP information is added, however, we note a dramatic increase in the number of rejected mechanisms. We attribute the discrepancy between our results and those of McLaughlin et al. (1983) to the fact that they appear to have relaxed the sP bounds by the use of an attenuation factor to account for large uncertainties in the S to P conversion at the free surface.

The effect of changing the takeoff angle from 20 to 40° was then examined for multiple stations, each separated by 60° in azimuth. As one would expect, each additional station reduced the number of consistent focal mechanisms. As before, the addition of sP amplitude information eliminated a significant number of mechanisms. These results are shown in Figure 17. The McLaughlin et al. (1983) results,

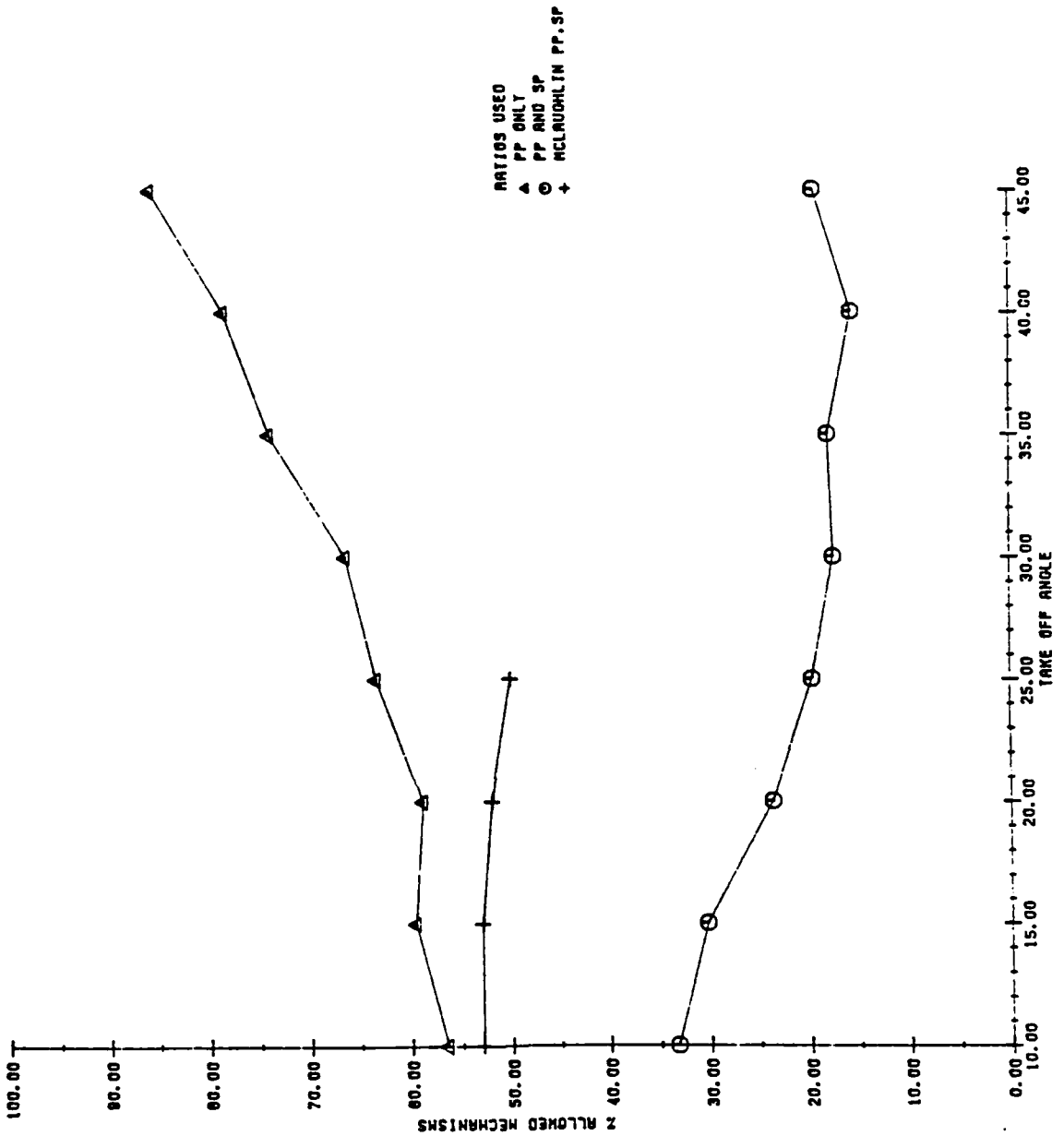

Figure 16. Discrimination ability of the Pearce algorithm using one station, plotted as a function of take-off angle. The larger take-off angles are appropriate for stations at upper mantle distances. A total of 3888 focal mechanisms were searched (every 10 degrees in slip, every 10 degrees in dip, and every 30 degrees in strike). The plus signs indicate results from McLaughlin et al. (1983) when both pP and sP amplitudes are restricted to be less than the P. The triangles indicate our pP only results and the circles indicate our results when both pP and sP are included.

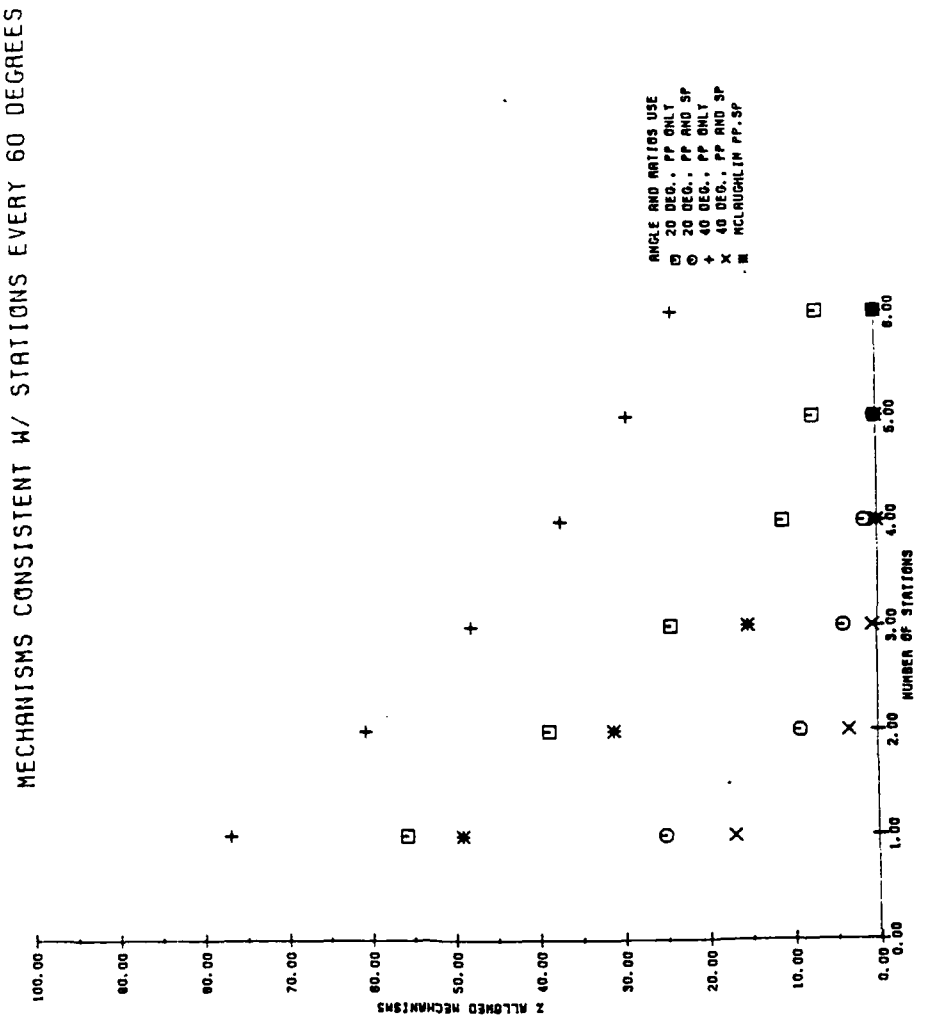

Figure 17. Discrimination ability of the Pearce algorithm for stations at 20 and 40 degree P-wave take-off angle, plotted as a function of the number of stations. Each added station is 60 degrees in azimuth from the previous station. The total number of focal mechanisms considered in our work was 3888. The asterisks indicate the results from McLaughlin et al. (1983) using both pP and sP information for stations at 20 degrees take-off angle. The squares and circles indicate our results at this take-off angle using pP/P amplitudes only and both pP/P and sP/P amplitudes. The pluses and crosses are similar except that they are for a typical upper mantle P-wave take-off angles of 40 degrees.

using pP and sP with a 20 degree P takeoff angle, are shown for comparison. To check our results we repeated the experiment for the same takeoff angle using pP information only and both pP and sP information. We also show our results, again for both the pP only and the combined pP and sP cases, using a P takeoff angle of 40°. When both phases are considered, it appears that 3 to 4 well distributed stations are sufficient to eliminate all possible focal mechanisms.

Multiple copies of the direct P-wave, generated in the upper mantle, can be mistaken for the reflected phases, pP and sP, that the Pearce algorithm relies on. The most desirable method of dealing with this complexity would be to accurately model and remove the upper mantle arrivals. This is currently unfeasible because the lateral heterogeneity in the upper mantle is extensive and poorly understood. The travel time and amplitude variations cannot be constrained accurately enough to reliably deconvolve the upper mantle response. An alternative is to completely avoid all data for which the pP and sP times are likely to coincide with an upper mantle arrival. A set of avoidance windows was determined from synthetics made using King and Calcagnile's (1976) upper mantle model KCA and from observations of actual Soviet explosions recorded at European and Asian stations (Figure 13). These windows were used in ascertaining the combinations of event depth and station distance that could be used in the Pearce algorithm with minimal contamination. The results are shown in Figure 18, which displays event depth in kilometers plotted against station distance in degrees. U's indicate unresolved areas where the

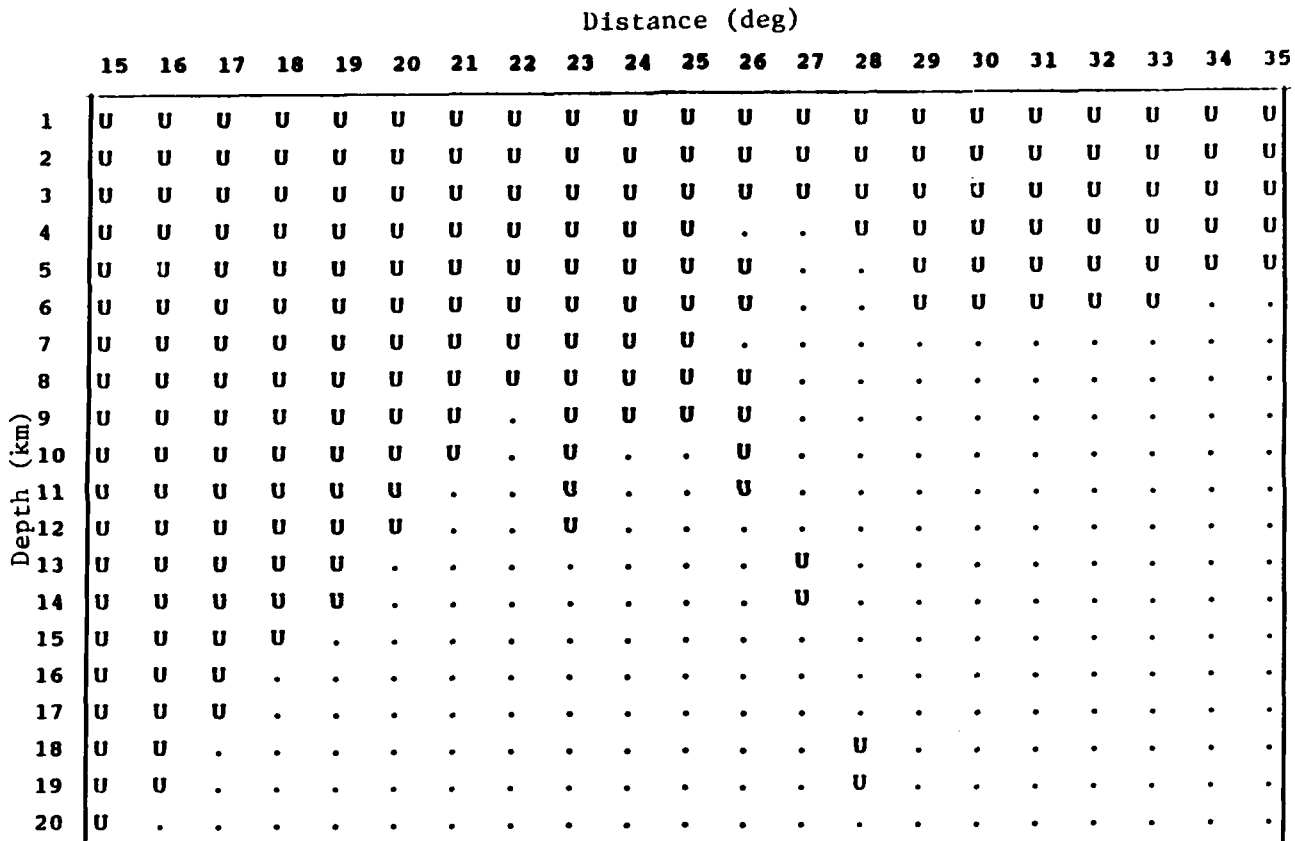

Figure 18. Resolvability of depth phases pP and sP as a function of event depth and station distance. Depths vary from 1 to 20 kilometers. Distances vary from 15 to 35 degrees. The U's indicate areas of unresolvability where upper mantle arrivals are expected at the same time as the reflected phases pP and sP.

reflected phases and the upper mantle arrivals are in conflict. In general, for stations greater than 21°, events deeper than 10 kilometers can be distinguished. The closer stations provide especially poor resolution because they typically have emergent first arrivals that hinder the alignment of those records and, correspondingly, extend the areas of possible conflict. However, the P_{CD} phase is very reliable in this region. If it can be identified, then depth phases associated with it may help resolve shallower events.

In summary, it appears that, in principle, the Pearce algorithm can be extended to upper mantle distances. As usual, good station coverage is essential. Also, good phase coverage, meaning the inclusion of both pP and sP information, is critical. Finally, some of the limitations at these distances are that earthquakes less than 5 kilometers deep may not be discriminated and that, for earthquakes in the 5 to 20 kilometer range, the shallower events can only be discriminated with information from the more distant stations (e.g. events shallower than 10 km require information from stations further than 26°).

5.0 Pearce Focal Sphere Analysis of Two Western US Events

Currently, one of the most important methods of discriminating between earthquakes and explosions is to conclusively demonstrate the presence of depth phases, pP and sP, indicating a hypocentral depth of greater than a few kilometers. The goal of our research is designed to decrease the size, depth, and distance at which these phases can be identified. Our primary emphasis has been on reducing the recording distance from teleseismic to upper mantle distances and therefore, we sought to model well recorded, previously studied events in the 10^{o} to 35^{o} distance range.

We present results from two events that fit this criteria. One event occurred in Wyoming on October 18, 1984; the other occurred in Idaho on October 29, 1983. Because of the proximity of several GDSN and RSTN stations, North America is an excellent location to pursue such an investigation. For both events, we began by associating observed arrivals with phases expected from published models of the upper mantle for the region. After settling upon one or more interpretations, we determined those focal mechanisms consistent with the observations. To accomplish this, we implemented a grid search over the entire range of possible mechanisms using the method proposed in the reports by Pearce (1977, 1979, 1980).

Briefly, for each possible focal mechanism, the predicted amplitude ratios for the phase pairs pP/P, sP/P, and sP/pP are computed for the

distance and azimuth of each station. These synthetic amplitude ratios are then compared with the observed amplitude ratios. Focal mechanisms that result in amplitude ratios that do not agree with the data are discarded. The successful mechanisms are typically displayed either on vector plots or on focal plane plots. Because polarity information was not included in our study, the number of acceptable focal mechanisms is at least twice as large as it might be had polarity data been available. The acceptable focal mechanisms can then be used for generating synthetics to compare against the original data.

The first event that we studied is the magnitude 5.4 (mb) that occurred on October 18, 1984 in the Laramie Mountains about 50 km southwest of Douglas, Wyoming. Seismograms for this event recorded at the RSTN (Regional Seismic Test Network) stations of RSON and RSNY and at the WWSSN (World Wide Standard Seismic Network) stations of SCP and COL are shown in Figure 19. The distances range from 12^{o} (1315 km) to 32^{o} (3630 km). The RSTN stations both show a strong, remarkably simple arrival, simpler than many observations of explosions at teleseismic distances. This simplicity allowed us to develop several interpretations with very tight bounds on the maximum relative amplitudes of the depth phases. Thus the two RSTN stations were used to direct our modeling efforts.

The time separation between the small first and large second arrivals is roughly 8 seconds for both RSON and RSNY, despite an 11^{o} (1200 km)

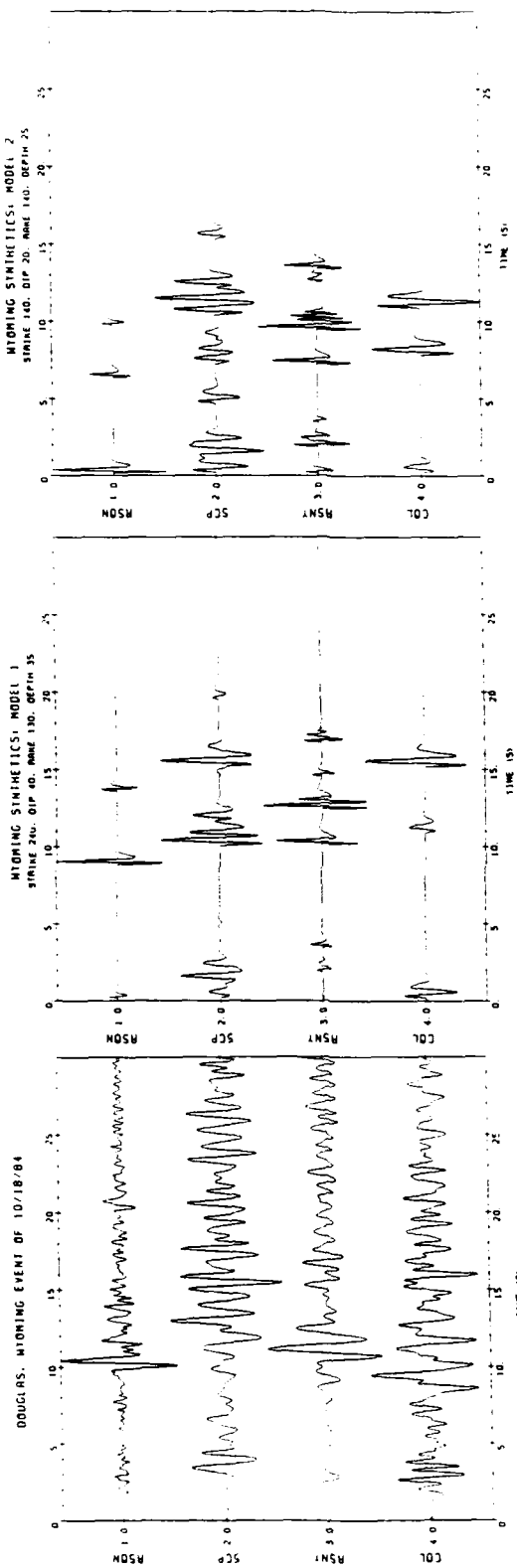

Figure 19. Data and synthetics for the October 18, 1984, Wyoming event (lat. 42.38, lon. -105.72). Stations distances in degrees are: RSON 11.8 (1315 km), SCP 20.9 (2320 km), RSNY 22.7 (2522 km), and COL 32.6 (3631 km). Model 1 assumes that the large second arrival at RSON and RSNY is pP. Model 2 assumes that the large second arrival at RSON is an upper mantle P with pP coming later back in the record, and the large second arrival at RSNY is pP.

difference in distance. The Upper mantle arrivals tend to move either forward or backward in the record as the epicentral distance is increased. The P - pP time delay, however, depends almost exclusively on the depth of the event and is less sensitive to the distance. This is the basis for our first interpretation: the small first arrival is P and the large second arrival is pP at both RSON and RSNY.

The upper mantle model, HWNE, for the western US was developed by Helmberger and Wiggins (1971). At 12°, the distance to RSON, this model predicts a small first arrival followed in 6 to 12 seconds by a large second arrival. This observation leads to our second interpretation: the first and large second arrivals at RSON are Pn and P with pP coming some time later in the record; as before, at RSNY, the first arrival is P and the large second arrival is pP.

Amplitude ratios were measured based on these two interpretations and the Pearce algorithm grid searches were performed. The resulting vector plots are shown in Figure 20. Given that data from only two stations were used, it is remarkable that such a small set of possible focal mechanisms is permissible. A few acceptable focal mechanisms for each model were then used to make synthetics appropriate for all four stations. These synthetics were generated by convolving together a series of spikes representing P, pP, and sP, a spike series based on the upper mantle arrivals predicted by the HWNE model, an instrument response, and an attenuation function with T^{*} (T/Q) = 0.2.

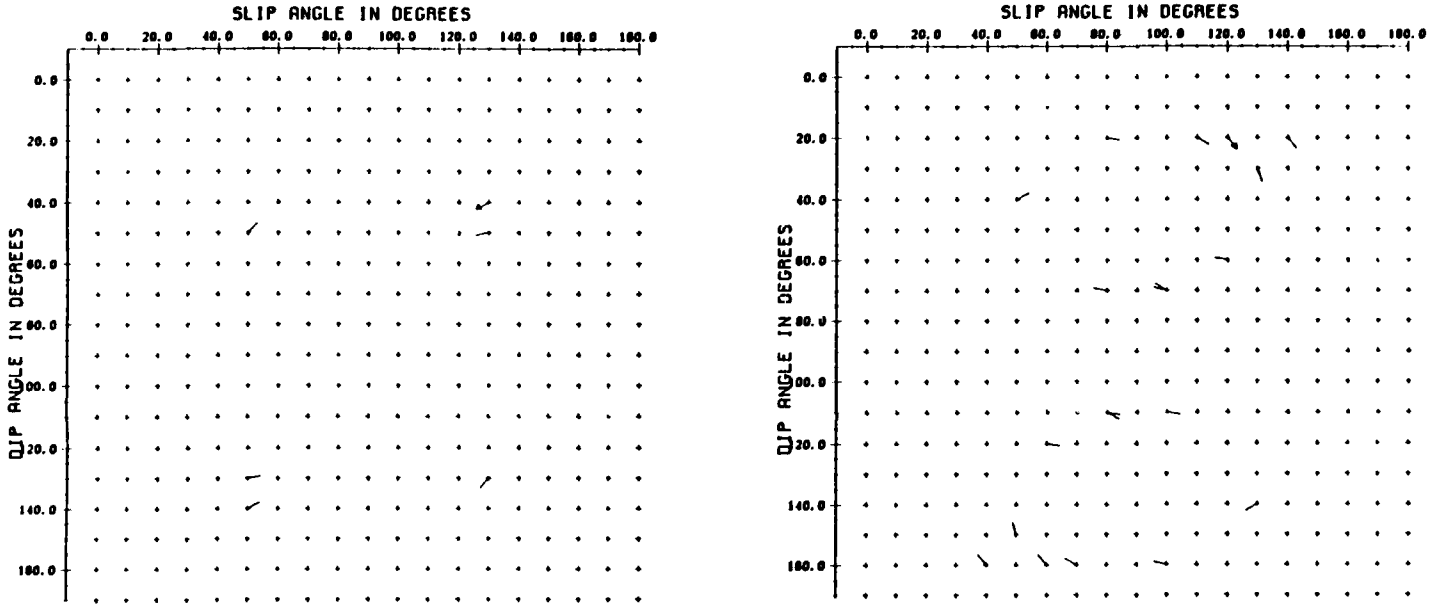

Figure 20. Vector plots of acceptable focal mechanisms as determined from the Pearce algorithm grid search for the Wyoming event. Polarity was not included so the plots look quite symmetric and the number of acceptable mechanisms has been doubled. Searched slip angles range from 0 to 180 and searched dip angles range from 0 to 180. Strikes, searched in increments of 20 degrees, range from 0 to 360 and are displayed by the clockwise orientation of the plotted vector as measured from 0 pointing vertically upwards. The vector with arrowhead indicates mechanism used to generate synthetics. The Pearce algorithm search was done using amplitude ratio measurements from RSON and RSNY. Results for model 1 are on the left, those for model 2 are on the right.

The best set of synthetics for each interpretation is shown in Figure 19 where they may be compared with the original data. The preferred mechanism for model 1 (large arrival is depth phase at both RSON and RSNY) is strike = 240°, dip = 40°, rake = 130°, and depth = 35 km. The preferred mechanism for model 2 (large arrival at RSON is upper mantle P, RSNY is the same as in model 1) is strike = 140°, dip = 20°, rake = 140°, and depth = 25 km. Although neither of these mechanisms match the data exactly, they both adequately match the major features in terms of both timing and relative amplitudes.

Finally, we compared our results with those of Langer, Martin, and Wood (1985). They found, based on aftershocks, a depth of 20 to 25 km and a nearly horizontal T axis that trended roughly N 35 E. This depth is in agreement with our model 2 solution of 25 km. The northeast trending tension axis is also consistent with the orientation of the fault planes for model 2 that are displayed on a focal plane plot in Figure 21.

The second event in our study is the magnitude 5.4 (m_b) aftershock that followed, by about a day and a half, the magnitude 6.2 (m_b) Borah Peak earthquake that occurred on October 28, 1983 along a segment of the Lost River fault between the Idaho towns of Challis and Mackay. Idaho seismograms for this aftershock, recorded on the RSTN stations of RSON, RSNT, and RSCP, are shown in Figure 22. The distances range from 15° (1700 km) to 23° (2600 km).

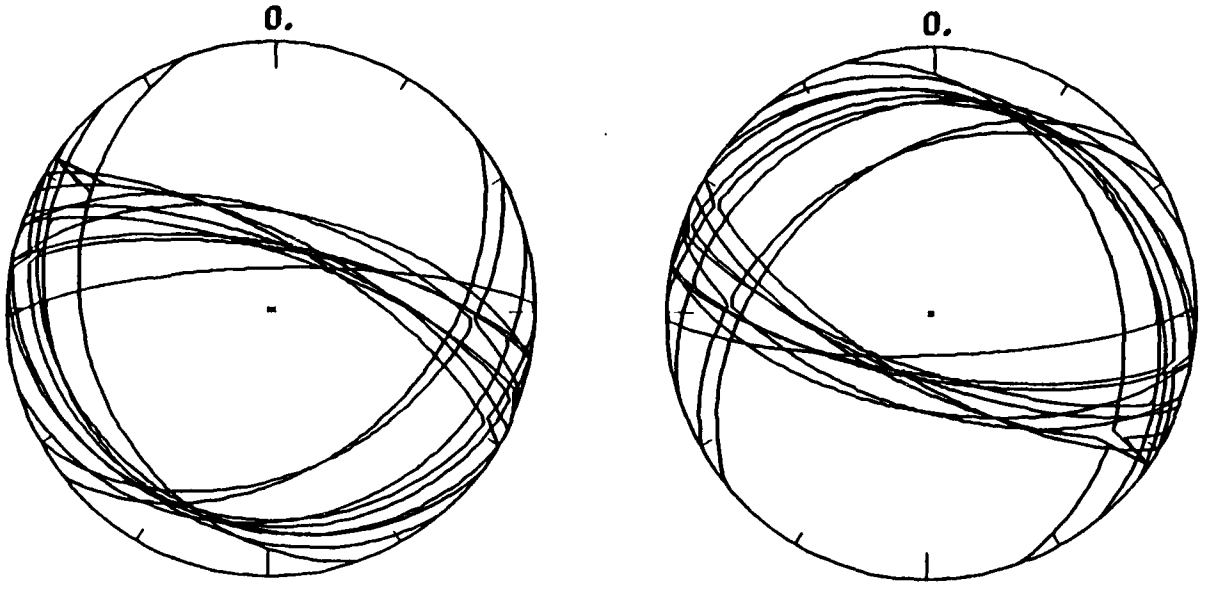

Figure 21. Focal plane plots of the acceptable mechanisms for model 2 for the Wyoming event. A lower hemisphere projection is on the left, and an upper is on the right. The majority of the mechanisms are consistent with a nearly horizontal tension axis oriented roughly NE.

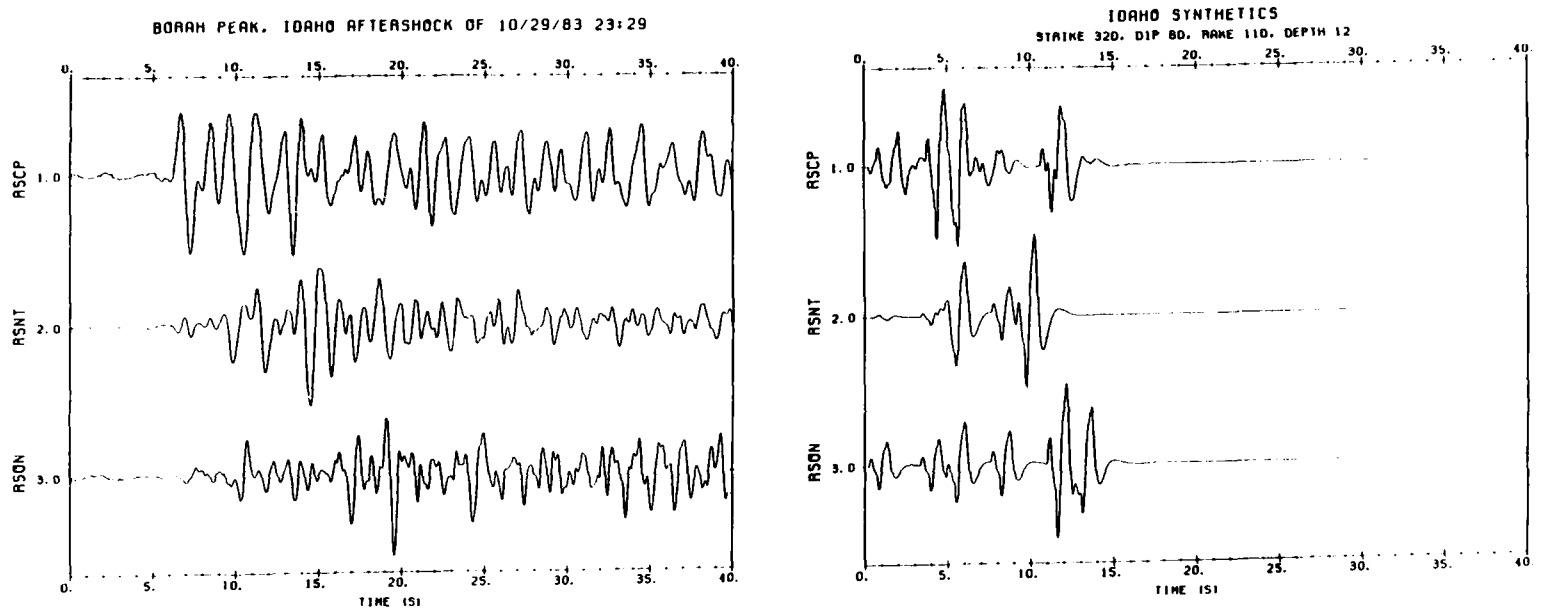

Figure 22. Data and synthetics for the October 29, 1983, Borah Peak, Idaho, aftershock of 23:29 (lat. 44.23, lon. -114.11). Stations distances in degrees are: RSON 15.3 (1701 km), RSNT 18.3 (2035 km), and RSCP 23.4 (2602 km).

In determining the association between observed arrivals and predicted phases, we began by inspecting the records for some time interval between arrivals that remains constant from station to station and that, therefore, might indicate the P - pP delay. Looking first at the RSNT record, one can see a second arrival which follows the first by about 3 seconds. This same 3 second delay can also be seen between the first two arrivals in the RSON record. In fact, it can be seen between the second and third and between the third and fourth arrivals at RSON as well. This periodicity should not be unexpected because stations at upper mantle distance may have as many as five copies of the P, pP, and sP phases and their delay times.

At 23°, the distance to RSCP, the HWNE upper mantle model predicts two or three arrivals within the first 2 to 3 seconds. Including the surface reflected pP and sP phases brings the arrival count up to at least 6 arrivals within the first 10 seconds. Because of this large amount of interference, we declined to make a specific interpretation for RSCP and instead allowed large bounds on the amplitudes of all three phases. At 18°, the distance to RSNT, the HWNE model predicts that the second upper mantle arrival will come about 3 seconds back in the record. Our interpretation for RSNT is that the first arrival is P and the second arrival is a combination of pP, sP, and the second copy of P. The largest arrival is then the combination of the second copies of pP and sP. At 15°, the distance to RSON, the HWNE model predicts that the second upper mantle arrival will come about 6 to 7 seconds back in the record. Therefore, we interpret the first two arrivals at

RSON to be P and pP, the next arrival to be an interfering combination of sP and the second copy of P, and the two largest arrivals to be the second copies of pP and sP.

We used this set of interpretations as a guide in measuring amplitude ratios that were then input into a Pearce algorithm grid search. Because of the interference effects that we expect to occur at all three stations, we allowed very generous bounds on these ratios. For this example, a large number of focal mechanisms are consistent with these ratios and are displayed as a vector plot in Figure 23.

About a dozen representative mechanisms were selected and used for making synthetics. These synthetics were generated as for the Wyoming event, but also include a triangular source function with a 1 s duration. The best matching set of synthetics is shown in Figure 22. It represents the response to an earthquake with strike = 320^{o}, dip = 60^{o}, rake = 110^{o}, and depth = 12 km. Although it models the general character of the data, it clearly is not a wiggle for wiggle match. In particular, it appears that the HWNE upper mantle model predicts a slightly larger delay, by about .5 to 1 second, between the first and second copies of the P, pP, and sP phases. Also, it should be noted that the relative amplitudes of the upper mantle branches are very uncertain. Despite these reservations, however, the synthetics do match the observations adequately enough to justify the possibility that the solution is the correct one.

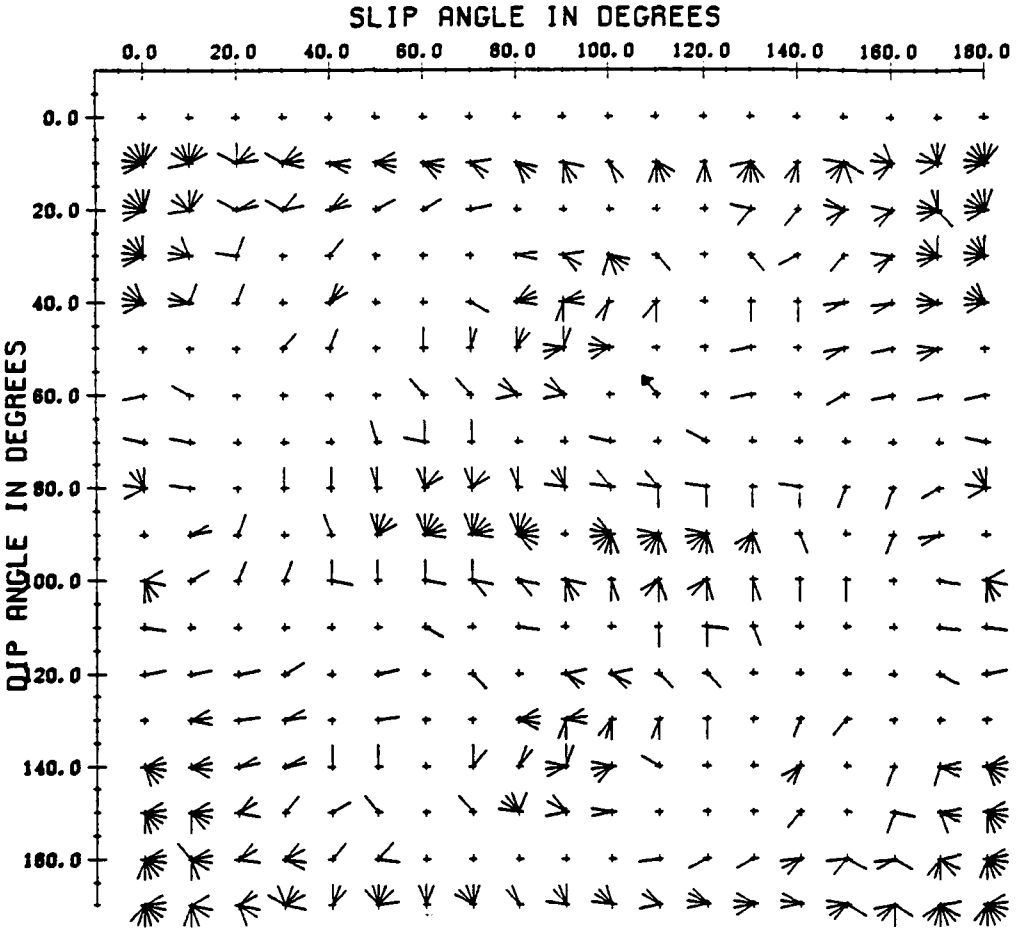

Figure 23. Vector plots of acceptable focal mechanisms as determined from a Pearce algorithm grid search for the Idaho event. See Figure 20 for a detailed description of this style of plot. The vector with arrowhead indicates mechanism used to generate synthetics.

This aftershock has been studied by Boatwright (1985) and Richins et al. (1987). Boatwright finds an average mechanism, using this and other similar aftershocks, of roughly strike = 324°, dip = 51°, rake = -70, and depth = 12.5 km. Richins et al. find a mechanism of strike = 309°, dip = 51°, rake = -65°, and depth = 10 km. Note, however, that this depth has been constrained. Our preferred mechanism of Figure 22 is similar to both of these published mechanisms.

In summary, our modeling of the Wyoming event of October 18, 1984 has demonstrated that this event is consistent with an earthquake occurring at a depth of 30 ± 5 km. Our modeling of the Borah Peak, Idaho aftershock of October 29, 1983 (23:29) has demonstrated that this event is consistent with an earthquake occurring at a depth of approximately 12 km. These results show that seismograms from upper mantle distances can be of use in constraining the focal mechanism of seismic events. However, this analysis also indicates that phase association of depth phases and the direct P- phases can be an extremely difficult and non-unique task.

6.0 Characterizing the Relative Amplitudes and Polarities of Later Arrivals by Filtering the Autocorrelation

As we have discussed, the application of the Pearce algorithm using data at upper mantle distances is complicated by the interference of the depth phases and the upper mantle refracted arrivals. At teleseismic distances, identification of depth phases is often a subjective process in which several stations are visually compared to see if later arrivals have the proper timing to be surface reflections. This visual correlation should be effective at upper-mantle distances as well since over a range of distances, the changes in relative timing of the upper-mantle arrivals are much more rapid than the change in timing of the depth phases. However, the required resolution on the timing of the arrivals is often distorted by the unknown source time function and some sort of processing is necessary to estimate and remove the effects of the source wavelet.

Another goal is the estimation of the polarity of the later arrivals, either absolute or relative to other P arrivals. The detection of polarity reversals can be very useful in discrimination methods, including the Pearce processor discussed earlier. Normally, the determination of polarity is done by observing the first motion of an arrival; this typically requires a large signal to noise ratio and is often difficult to apply to later arrivals. Another strategy, presented by Smart and McLaughlin (1985) is to correlate the initial P wave with the remainder of the P- wave to locate the time and estimate

the polarity of the pP phase. Smart and McLaughlin (1985) also correlate the P and pP wavetrains at different stations to estimate the polarities over a global network.

The large variation in the amplitudes and arrival times of the triplicated phases from the upper mantle structure precludes using a direct deconvolution technique to isolate the depth phases from the upper mantle arrivals. Processing techniques, designed to clean up the data using band-pass filtering, stacking, or polarization filtering, only marginally improve the situation, although the signal enhancement provided by these techniques is valuable for increasing overall signal to noise characteristics. Ideally, we would like a method to extract from the seismogram the source wavelet and the wavetrain of spike-like arrivals that are the upper-mantle arrivals and the depth phases. The results of such a processing technique would be a high resolution trace composed of the upper mantle refracted arrivals and the depth phases associated with each upper mantle arrival. Using this deconvolved spike train of arrivals with its higher resolution in time, a visual correlation would be more successful in picking out the surface reflections and constraining their amplitudes and polarities.

Separating a source wavelet from a wavetrain of "spike-like" arrivals is a fundamental and recurring problem in observational seismology. We start with a simple model of the seismogram:

$$u(t) = s(t) * \sum_i \{ (e_i(t,p_i) * d_i(t,p_i) * q_i(t) \} \qquad (1)$$

where $s(t)$ is the source time function, $e_i(t,p_i)$ is the ith refracted arrival from the upper mantle with ray parameter (or slowness) p_i, $d_i(t,p_i)$ is the sequence of P, pP, and sP phases that have been refracted along the propagation path characterized by $e_i(t,p_i)$, and $q_i(t)$ is the attenuation function for the ith upper mantle arrival. As we have seen, global earth models predict as many as five arrivals from the upper mantle, which imply very complicated seismograms.

Deconvolution methods to separate an unknown source wavelet from an unknown spike wave train require some constraints on both the source wavelet and spike sequence (e.g. Robinson and Treitel, 1980). A common constraint is that the source is minimum phase, which is not a reliable assumption for an earthquake source, which often occur as multiple events. A typical constraint on the spike sequence is that it is random and stationary. The number of arrivals in the seismogram is too few for this assumption to be valid. Thus, the standard wavelet processing techniques that are available to the exploration geophysicists do not give good results except in simple cases.

An attractive alternative is to give up (initially) on finding the spike wave train of upper-mantle arrivals and depth phases and concentrate on looking for timing and polarity systematics in the autocorrelation of the observed seismograms. If we can devise a wavelet extraction method (or spiking filter) to enhance the resolution of correlated arrivals in the autocorrelation function, then we may hope

to see some features that separate some explosion observations from many of the earthquake seismograms. In the following, we will outline the proposed method and give some preliminary results using synthetics and actual observations. Current research is concentrated on applying the methods to a large suite of observed data and the results will be presented in a subsequent report.

To devise our spiking filter for the autocorrelation function, we make some additional simplifying assumptions to our convolutional model in Equation 1. One further assumption is that the difference in the attenuation between the different upper-mantle branches is negligible. This is justified by the work presented in Der et al. (1986) in which they determined the differential t* for the major branches of the upper mantle arrivals in western Eurasia. With this assumption, we can separate the frequency dependent part of Equation 1 in to the effective source wavelet, $s_e(t)$, where

$$A(t) = s_e(t) \odot s_e(t) * k(t) \odot k(t). \qquad (2)$$

In Equation 2, A(t) is the autocorrelation function, k(t) is the spike wavetrain, and $\odot$ denotes correlation. Our final assumption is that the windowed autocorrelation, $A_w(t)$, windowed symmetrically about t=0, is an approximation of the autocorrelation of the effective source. This windowing is implemented in the frequency domain by smoothing the power spectrum, typically with a boxcar or exponential, and by dividing the original power spectrum by the result. Thus, we have

$$A_w(f) = S(f) * A(f) \qquad (3)$$

where f denotes frequency and S(f) is the smoothing operator.

Finally,

$$A_k(f) = A(f) \; / \; A_w(f) \qquad (4)$$

where $A_k(t)$ is the autocorrelation of the spike arrival sequence.

As examples, we show results from a synthetic test in Figure 24. The test was generated by summing three sets of P, pP, and sP arrivals at lag times at 4.75 and 7 s similar to those typically encountered in seismograms at upper-mantle distances. Each set of arrivals had a different attenuation function associated with them (t* = 0.25, 0.30, and 0.35) and slightly different moveouts for pP, and sP to account for the different takeoff angles at the source. The resulting autocorrelation function of the spike arrival sequence is complex, but in general shows only a few large spikes, one of which corresponds to correlation between different depth phases associated with different upper-mantle arrivals and the other corresponding to the pP - P delay time of approximately 3.5 s. Relative polarity information is preserved, however poor signal to noise ratio for the different arrivals in the P coda will often make this information suspect.

Figure 25 is an example of an actual explosion recorded at 19.8^{o} with clear later arrivals that have well defined polarity. On the autocorrelation and filtered autocorrelation traces, the major arrivals stand out and there is no indication of any significant polarity reversal, yet the relative polarities of the arrivals are not definite. The arrivals are more distinct on the original trace and the correlation traces show possibly significant correlations near 4 and 10 s. As a single station analysis tool, the method probably provides no more new

information but if we consider multiple stations, at different azimuths and distances, we anticipate that some simple stacking techniques may prove useful for detecting and enhancing depth phases from shallow events when the seismograms are complicated by upper mantle triplications.

Clearly, this is a preliminary outline of a method that requires further testing by application to data with multiple station coverage and we will present the results in the next report. The method is closely related to a cepstral method, which has shown some preliminary promise for enhancing depth phases in complex seismograms (Alexander, 1987). In the cepstral method, the operation of taking the logarithm of the spectra has a similar purpose to our filtering process. We need to devise an objective means of isolating a "significant" arrival on the spiked autocorrelation function. Also the length of auto-correlation of the effective source will affect the results and this should be explored further. By testing the method on actual data, we will address how the method behaves in the presence of noise. Finally, we need to apply the method to as many explosions as are available to determine a false alarm threshold. The results of applying the method to a large suite of explosions can then be compared to results from a large suite of earthquakes to see if the method has useful discrimination applications.

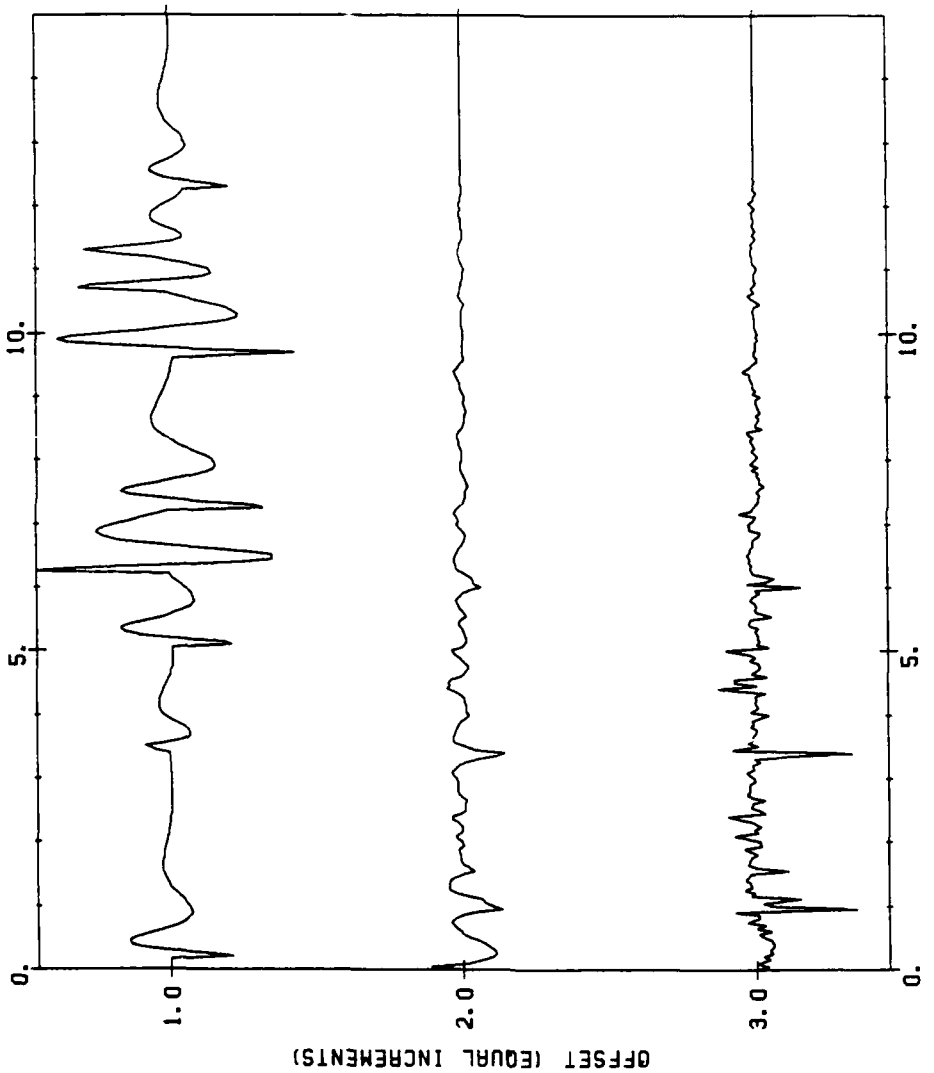

Figure 24. Synthetic example demonstrating how filtering the autocorrelation function enhances arrivals. Top trace is a synthetic seismogram, middle trace is autocorrelation function (positive time only) and bottom trace is filtered autocorrelation.

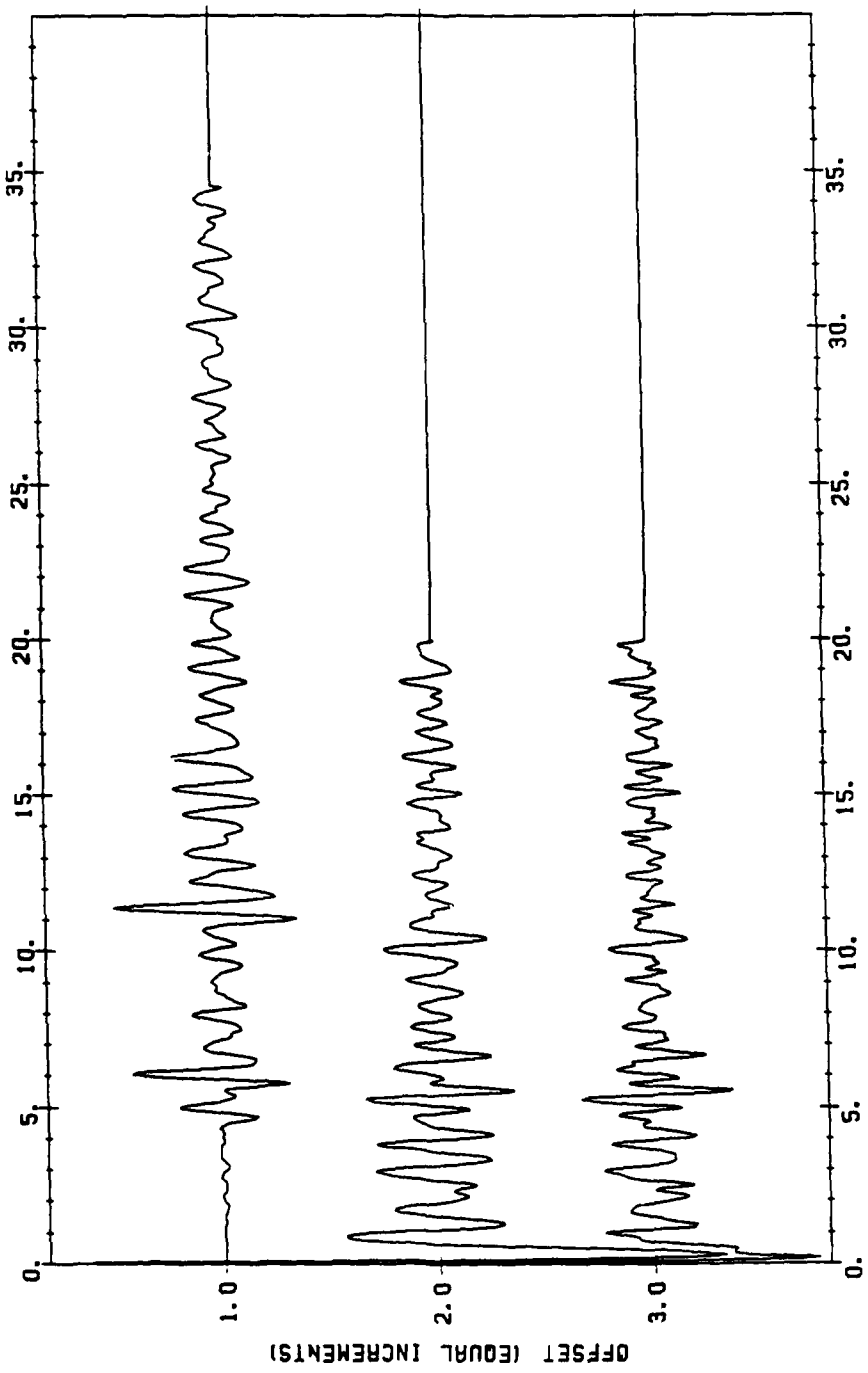

Figure 25. Seismogram, autocorrelation, and filtered autocorrelation for a MAIO recording of an East Kazakh explosion (19.8°). The time window for the autocorrelation is 30 s, which introduces substantial noise into the autocorrelation. The dominant arrivals are still visible and can be compared with additional stations for similarities.

7.0 Conclusions and Recommendations

A technique, such as the Pearce algorithm, that interprets the complexity in the P-wave train in terms of the depth phases, pP and sP, and a double couple radiation pattern should, theoretically, have good discrimination properties. Explosions, due to their shallow depth, have a simplicity that should be recognizable when observed over a wide range of azimuths. At upper-mantle distances, 15^{o} to 30^{o}, the P-waves are more complex, but, if the propagation path can be regionalized and calibrated, the major arrivals from the triplication branches can be recognized and separated from additional arrivals that may be potential depth phases. The high velocity gradients in the upper mantle tend to focus the body-wave energy at these distances. If the attenuation in the uppermost mantle is low, which is believed to be the case for some continental regions, then the P-wave amplitudes are a factor of 3 to 4 times larger from 15^{o} to 25^{o} than they are beyond 27^{o}.

While explosions are simple enough such that a double couple mechanism is incompatible with observations in three quadrants, earthquakes are sufficiently complex that isolating depth phases and using relative amplitude data to constrain the focal mechanism is difficult.

The observations presented in this paper suggest that a multi-station complexity measure may be useful as a discrimination tool at these distances. Complexity is a vague concept and, ultimately, may not be

simply parameterized. We may want to measure it by observing average amplitude in some arrival window relative to an initial arrival window as reviewed in Douglas (1981). Alternatively, the Pearce algorithm suggests that we search for discrete later arrivals that correlate between several seismograms, which may suggest other possible measures.

The complexity observed in earthquake seismograms is not completely understood but is likely related to S to P scattering in addition to depth phases. At upper-mantle distances, a complex coda, generated in the source region, constructively adds at the receiver. Explosions tend to be much simpler, with discrete arrivals that can be predicted if the regional structure is known. Even those explosions that appear to be complex, such as discussed by Douglas (1981), are usually associated with anomalous attenuation of a direct arrival, as opposed to strong heterogeneities at the source. Such problems, and others associated with the tremendous variation in high-frequency observations, may be alleviated by the multi-station approach. Several definitions of complexity may be necessary and these will probably need to be calibrated for individual station and source regions, much as instruments and sites are currently calibrated.

The performance of any of these waveform interpretation methods for the small events of interest in a treaty monitoring program cannot be fully evaluated with the limited amount of high quality digital data available. Both our work and previous studies have indicated that good data coverage is essential to the analysis. For the small events

of interest, some signal processing will almost certainly be necessary, which requires 3 component data or small arrays. Until these data are available, many conclusions are premature and may be overly pessimistic about the potential of these methods.

8.0 References

Alexander, S.S., L.Tang, A. Borkowski, and D. Stockar, 1987 The use of propagation-corrected Lg Spectra to estimate yields of Soviet explosions and isolation and enhancement of regional phases for earthquakes in the Eastern United States, (abstr). Presented at 9th annual DARPA/AFGL seismic research symposium

Boatwright, J., 1985, Characteristics of the aftershock sequence of the Borah Peak, Idaho, earthquake determined from digital recordings of the events, Bull. Seism. Soc. Am. 75, 1265-1284

Der, Z.A., W.W. Chan, A.C. Lees and M.E. Marshall, 1986, Models of the frequency dependence of Q in the mantle underlying tectonic areas of North America, Eurasia and Eastern Pacific, TGAL 86-5, contract no. F08606-85-L-0023, Teledyne Geotech, Alexandria, Virginia

Douglas, A., 1981, Seismic source identification: a review of past and present research efforts, in Identification of Seismic Sources: Earthquake or Underground Explosion, E. Husebye and S. Mykkeltveit ed., D. Reidel: Dordrecht, Holland

Evernden, J.F., 1967, Magnitude determination at regional and near regional distances in the United States, Bull Seism. Soc. Am. 57, 591-639.

Given, J. W., and D.V. Helmberger, 1980, Upper mantle structure of northwest Eurasia, J. Geophys. Res. 85, 7183-7194.

Grand, S.P. and D.V. Helmberger, 1984, Upper mantle shear structure of North America, Geophys. J. 76, 399-438

Helmberger, D. and R.A. Wiggins, 1971, Upper mantle structure of Midwestern United States. J. Geophys. Res., 76, 3229-3245

King D.W. and G. Calcagnile, 1976, P-wave velocity in the upper mantle beneath Fennoscandia and Western Russia, Geophys. J. 46, 407-432

Langer, C.J., R.A. Martin, Jr. and C.K. Wood (1985). Preliminary results of the aftershock investigation of the October 18, 1984, Laramie Mountains, Wyoming, earthquake (abstract), Earthquake Notes 55, 24

Langston, 1982, Aspects of Pn and Pg propagation at regional distances. Bull Seis. Soc. Am 72, 457-472

McLaughlin, K.L., D.W. Rivers and M.A. Brennan, 1983, Pearce Focal Sphere analysis of explosion and earthquake mechanisms. TGAL-TR-83-4 contract no. F08606-79-C-0007; Teledyne Geotech, Alexandria, Virginia

McLaughlin, K.L., D.W. Rivers, M.E. Marshall and R.A. Wagner, 1985, Focal mechanism analysis as a method for teleseismic discrimination, in The Vela Program: A Twenty-Five Year Review of Basic Research, A.U. Kerr, ed. 735-740.

Pearce, R.G., 1977, Fault plane solutions using relative amplitudes of pP and P. Geophys. J. 50, 381-394.

Pearce, R.G., 1979, Earthquake focal mechanisms from relative amplitude of P, pP and sP: method and computer program, AWRE Report 0-41/79, Blacknest, Berkshire, England.

Pearce, R.G., 1980, Fault plane solutions using relative amplitudes of P and surface reflections: further studies. Geophys. J. 60, 159-157

Rial J.A., S. Grand and D.V. Helmberger, 1984, A note on lateral variation in upper mantle shear-wave velocity across the Alpine Front. Geophys. J., 77, 639-654.

Richins, W.C., J.C. Pechmann, R.B. Smith, C.J. Langer, S.K. Goeter, J.E. Zollweg and J.J. King 1987. The 1983 Borah Peak, Idaho, earthquake and its aftershocks, Bull Seismol. Soc. Am. 77, 694-723.

Robinson, E. & S. Treitel, 1980, Geophysical Signal Analysis. Englewood Cliffs, N.J.: Prentice-Hall Inc.

Smart, E. and K.L. McLaughlin, 1985, Discrimination by detection of the relative polarity of the entire P waveform. TGAL-85-12, contract no. FO 8606-85-C-0022, Teledyne Geotech, Alexandria, Virginia.

Thirlaway, H.I.S., 1966, Interpreting array records: explosion and earthquake P-wave trains which have traversed the deep mantle, Proc. R. Soc. Series A 290, 385-395.

Walck, M.C., 1984, The P-wave, upper mantle structure beneath an active spreading center: The Gulf of Calif., Geophys. J. 76, 697-724.

DISTRIBUTION LIST
FOR UNCLASSIFIED REPORTS
DARPA-FUNDED PROJECTS
(Last Revised: 15 Mar 88)

RECIPIENT	NUMBER OF COPIES
DEPARTMENT OF DEFENSE	
DARPA/NMRO ATTN: Dr. R. Alewine and Dr. R. Blandford 1400 Wilson Boulevard Arlington, VA 22209-2308	2
Defense Intelligence Agency Directorate for Scientific and Technical Intelligence Washington, DC 20340-6158	1
Defense Nuclear Agency Shock Physics Washington, DC 20305-1000	1
Defense Technical Information Center Cameron Station Alexandria, VA 22314	12
DEPARTMENT OF THE AIR FORCE	
AFGL/LWH ATTN: Mr. J. Lewkowicz Terrestrial Sciences Division Hanscom AFB, MA 01731-5000	1
AFOSR/NP Bldg. 410, Room C222 Bolling AFB, Washington, DC 20332-6448	1
AFTAC/DA (STINFO) Patrick AFB, FL 32925-6001	1
AFTAC/TT Patrick AFB, FL 32925-6001	3
AFWL/NTESG Kirkland AFB, NM 87171-6008	1

RECIPIENT	NUMBER OF COPIES

DEPARTMENT OF THE NAVY

NORDA
ATTN: Dr. J. A. Ballard
Code 543
NSTL Station, MS 39529 — 1

DEPARTMENT OF ENERGY

Department of Energy
ATTN: Mr. Max A. Koontz (DP-52)
International Security Affairs
1000 Independence Avenue
Washington, DC 20585 — 1

Lawrence Livermore National Laboratory
ATTN: Dr. J. Hannon, Dr. S. Taylor, and Dr. K. Nakanishi
University of California
P. O. Box 808
Livermore, CA 94550 — 3

Los Alamos Scientific Laboratory
ATTN: Dr. C. Newton
P. O. Box 1663
Los Alamos, NM 87544 — 2

Sandia Laboratories
ATTN: Mr. P. Stokes, Dept. 9110
P. O. Box 5800
Albuquerque, NM 87185 — 1

OTHER GOVERNMENT AGENCIES

Central Intelligence Agency
ATTN: Dr. L. Turnbull
OSI/NED, Room 5G48
Washington, DC 20505 — 1

U. S. Arms Control and Disarmament Agency
ATTN: Dr. M. Eimer
Verification and Intelligence Bureau, Rm. 4953
Washington, DC 20451 — 1

U. S. Arms Control and Disarmament Agency
ATTN: Mr. R. J. Morrow
Multilateral Affairs Bureau, Rm. 5499
Washington, DC 20451 — 1

RECIPIENT	NUMBER OF COPIES

OTHER GOVERNMENT AGENCIES (Continued)

U. S. Geological Survey — 1
ATTN: Dr. T. Hanks
National Earthquake Research Center
345 Middlefield Road
Menlo Park, CA 94025

U. S. Geological Survey MS-913 — 1
ATTN: Dr. R. Masse
Global Seismology Branch
Box 25046, Stop 967
Denver Federal Center
Denver, CO 80225

UNIVERSITIES

Boston College — 1
ATTN: Dr. A. Kafka
Western Observatory
381 Concord Road
Weston, MA 02193

California Institute of Technology — 1
ATTN: Dr. D. Harkrider
Seismological Laboratory
Pasadena, CA 91125

Columbia University — 1
ATTN: Dr. L. Sykes
Lamont-Doherty Geological Observatory
Palisades, NY 10964

Cornell University — 1
ATTN: Dr. M. Barazangi
INSTOC
Snee Hall
Ithaca, NY 14853

Harvard University — 1
ATTN: Dr. J. Woodhouse
Hoffman Laboratory
20 Oxford Street
Cambridge, MA 02138

Massachusetts Institute of Technology — 3
ATTN: Dr. S. Soloman, Dr. N. Toksoz, and Dr. T. Jordan
Department of Earth and Planetary Sciences
Cambridge, MA 02139

RECIPIENT	NUMBER OF COPIES
UNIVERSITIES (Continued)	
Southern Methodist University ATTN: Dr. E. Herrin and Dr. B. Stump Geophysical Laboratory Dallas, TX 75275	2
State University of New York at Binghamton ATTN: Dr. F. Wu Department of Geological Sciences Vestal, NY 13901	1
St. Louis University ATTN: Dr. O. Nuttli and Dr. R. Herrmann Department of Earth and Atmospheric Sciences 3507 Laclede St. Louis, MO 63156	2
The Pennsylvania State University ATTN: Dr. S. Alexander Geosciences Department 403 Deike Building University Park, PA 16802	1
University of Arizona ATTN: Dr. T. Wallace Department of Geosciences Tucson, AZ 85721	1
University of California, Berkeley ATTN: Dr. T. McEvilly Department of Geology and Geophysics Berkeley, CA 94720	1
University of California, Los Angeles ATTN: Dr. L. Knopoff 405 Hilgard Avenue Los Angeles, CA 90024	1
University of California, San Diego ATTN: Dr. J. Orcutt Scripps Institute of Oceanography La Jolla, CA 92093	1
University of Colorado ATTN: Dr. C. Archambeau CIRES Boulder, CO 80309	1

RECIPIENT	NUMBER OF COPIES
UNIVERSITIES (Continued)	
University of Illinois ATTN: Dr. S. Grand Department of Geology 1301 West Green Street Urbana, IL 61801	1
University of Michigan ATTN: Dr. T. Lay Department of Geological Sciences Ann Arbor, MI 48109-1063	1
University of Nevada ATTN: Dr. K. Priestley Mackay School of Mines Reno, NV 89557	1
University of Southern California ATTN: Dr. K. Aki Center for Earth Sciences University Park Los Angeles, CA 90089-0741	1
DEPARTMENT OF DEFENSE CONTRACTORS	
Analytical Sciences Corporation, The Dr. Richard Sailor ATTN: Document Control 55 Walkers Brook Drive Reading, MA 01867	1
Applied Theory, Inc. ATTN: Dr. J. Trulio 930 South La Brea Avenue, Suite 2 Los Angeles, CA 90036	1
Center for Seismic Studies ATTN: Dr. C. Romney and Mr. R. Perez 1300 N. 17th Street, Suite 1450 Arlington, VA 22209	2
ENSCO, Inc. ATTN: Mr. John R. Stevenson P. O. Box 1346 Springfield, VA 22151	1

RECIPIENT	NUMBER OF COPIES

DEPARTMENT OF DEFENSE CONTRACTORS (Continued)

ENSCO, Inc. 1
ATTN: Dr. R. Kemerait
445 Pineda Court
Melbourne, FL 32940-7508

Gould, Inc. 1
ATTN: Mr. R. J. Woodard
Chesapeake Instrument Division
6711 Baymeadow Drive
Glen Burnie, MD 21061

Maxwell Laboratories, Inc. 1
S-CUBED Reston Geophysics Office
ATTN: Mr. J. Murphy, Suite 1112
11800 Sunrise Valley Drive
Reston, VA 22091

Pacific Sierra Research Corp. 1
ATTN: Mr. F. Thomas
12340 Santa Monica Boulevard
Los Angeles, CA 90025

Rockwell International 1
ATTN: B. Tittmann
1049 Camino Dos Rios
Thousand Oaks, CA 91360

Rondout Associates, Inc. 1
ATTN: Dr. P. Pomeroy
P. O. Box 224
Stone Ridge, NY 12484

Science Applications International Corporation 1
ATTN: Document Control (Dr. T. Bache, Jr.)
10260 Campus Point Drive
San Diego, CA 92121

Science Horizons 2
ATTN: Dr. T. Cherry and Dr. J. Minster
710 Encinitas Blvd., Suite 101
Encinitas, CA 92024

Sierra Geophysics, Inc. 2
ATTN: Dr. R. Hart and Dr. G. Mellman
11255 Kirkland Way
P. O. Box 3886
Kirkland, WA 98124

RECIPIENT	NUMBER OF COPIES
DEPARTMENT OF DEFENSE CONTRACTORS (Continued)	
SRI International ATTN: Dr. A. Florence 333 Ravensworth Avenue Menlo Park, CA 94025	1
Teledyne Industries, Inc. Teledyne Geotech Alexandria Laboratories ATTN: Mr. W. Rivers 314 Montgomery Street Alexandria, VA 22314-1581	1
Woodward-Clyde Consultants ATTN: Dr. L. Burdick P. O. Box 93254 Pasadena, CA 91109-3254	1
NON-U.S. RECIPIENTS	
Blacknest Seismological Center ATTN: Mr. Peter Marshall Atomic Weapons Research Establishment UK Ministry of Defense Brimpton, Reading RG7-4RS United Kingdom	1
National Defense Research Institute ATTN: Dr. Ola Dahlman Stockholm 80, Sweden	1
NTNF NORSAR ATTN: Dr. Frode Ringdal P. O. Box 51 N-2007 Kjeller Norway	1
OTHER DISTRIBUTION	
To be determined by the project office	0
TOTAL	91

END
DATED
FILM
8-88
DTIC